The effect of changing cone apex angle on the velocity & geometry of

Shaped Charge Jets

Arun Sherlock

2318644

30/12/2025

—

Kelvin Donne

—

Advanced Physics of OME

Contents

1. Abstract 5
2. Introduction 6
2.1 Shaped Charge Concept 6
2.1.1 What is a Shaped Charge? 6
2.2 Shaped Charge 7
2.2.1 Overview 7
2.2.2 Civilian Applications 7
2.2.3 – Defence Applications 8
2.3 Shock Physics 9
2.3.1 - Introduction 9
2.3.2 – Euler Equations 9
2.3.3 – Rankine-Hugoniot Equations 9
2.3.4 – Rayleigh Line Relationship 10
2.3.5 – Jones-Wilkins-Lee Equation of State 10
3 Modelling Scope 11
3.1 Overview 11
3.2 Charge A 11
3.3 Charge B 11
4 Literature Review 12
4.1 Shaped Charge Modelling 12
4.1.1 – Introduction & Scope 12
4.1.2 – Geometry & Materials 12
4.1.3 – Validation of Jet Velocity 12
5. Modelling Setup 13
5.1 Material Properties 13
5.2 Meshing 13
5.3 Interactions & Fixtures 14
5.4 Limitations 14
6 Setup 15
6.2 General Setup 15
6.1.1 – Material Properties 15
6.1.2 – Interactions 15
6.1.3 – Mesh Type & Control 16
6.3 Charge 1 – 2D 16
6.2.1 – Parts, Properties & Assembly 16
6.2.2 – Meshing 17
6.4 Charge 2 – 2D 18
6.4.1 – Parts, Properties & Assembly 18

6.4.2 – Meshing 18
6.5 Charge 2 - 3D 19
6.5.1 – Parts, Properties & Assembly 19
6.5.2 – Meshing 19
7. Results 20
7.1 Charge 1 – 2D 20
7.2 Charge 2 – 2D 21
7.3 Charge 2 - 3D 22
8. Validation 23
9. Conclusion 24
10. References 25
11. Appendices 27
Appendix A – Interaction Setup 27
A-1 – Oxygen Free Copper 27
A-2– Aluminium 6061—T6 28
A-3 – Plastic Explosive 4 (PE4) 29
Appendix B – Technical Drawings 30
B-1 – Charge A 30
B-2 – Charge B 30
Appendix C – Interaction Definition 31
Appendix D – Charge 1, 2D Results 33
Appendix E – Charge 2, 2D Results 35
Appendix F – Charge 2, 3D Results 38

Intentionally left blank

Table of Figures

Figure	Content
1	An example of a shaped charge, with a copper liner [3].
2	HERO O-FRAC, an example of shaped charge uses in oil well fracking [6].
3	M830 High Explosive Anti-Tank (HEAT) Cross sectional Diagram [7].
4	Shaped charge and follow through bomb as used in AGM-154C [9].
5	Alfords Technologies Dioplex EOD (linear shaped charge) fitted onto UXO [10].
6	Hugoniots and Rayleigh Line [12].
7	JWL EOS Parameters for PE4.
8	Example of a meshed shaped charge.
9	Material properties, as used in simulation.
10	Element type selection.
11	Mesh control settings used.
12	Assembled 2D charge 1, with materials assigned.
13	Structured meshing used on the liner & HE fill.
14	Meshed Charge 1 2D.
15	Meshed charge 2, 2D.
16	Cone liner, 3 dimensional.
17	Casing, 3 dimensional.
18	HE Fill, 3 dimensional.
19	Meshed charge 2 – 3D.
20	Initial detonation point, Charge 1, 2D.
21	Comparative jet [15].
22	Charge 1 Jet geometry.
23	Velocity, tip of jet, charge 1, 2D.
24	Pressure wave at initial & second time step.
25	Pressure wave at initial & second time step.
26	Charge 2, 2D Jet Velocity plot.
27	Jet Geometry, Charge 1 2D.
28	Jet Geometry, Charge 2 2D.
29	Excess distortion error, highlighted red.
30	Example of charge 2, 3D using SPH.
31	Unbounded SPH error.
32	Comparative Jet [15].
33	Jet Geometry, Charge 2, 3D.
34	Jet Velocity, Charge 2, 3D.
35	Jet tip velocity, comparative study [15].
36	Charge 1, 2D, Jet tip velocities.

Abbreviations

Abbreviation	Meaning
HEAT	High Explosive, Anti-Tank
BROACH	Bomb, Royal Ordnance, Augmenting Charge
EOD	Explosive Ordnance Disposal
UXO	Unexploded Ordnance
JWL	Jones-Wilkins-Lee
EOS	Equation of State
PE4	Plastic Explosive 4
RDX	Royal Demolition Explosive (Cyclotrimethylenetrinitramine)
CAD	Computer Aided Design
CAE	Computer Aided Engineering
SPH	Solid Particle Hydrodynamics
HE	High Explosive
2D	Two Dimensional
3D	Three Dimensional
EFP	Explosively Formed Penetrator
TNT	Trinitrotoluene

1. Abstract

A report considering the concept of shaped charges, including their discovery & historical development, leading into a simulation study, supported by literature review, into the effects of changing the cone angle (60° and 70°) on the velocity and shape of the jet formed, with validation provided from similar studies. The results of the study were of limited accuracy but provide an insight into the techniques used to model shaped charges, and potential improvements in both modelling and charge design. Both charges are filled with plastic explosive 4, with the aim of providing an example of a real-world user filled charge system. A wide range of methods to aid in the running of high stress simulations are trialled to find the most accurate method, with the best results.

2. Introduction

2.1 Shaped Charge Concept

2.1.1 What is a Shaped Charge?

A shaped charge is an explosive device with a hollow cavity on one face. This hollow cavity, which assumes different geometry depending on the intended use case, focuses and thus amplifies the energy of the detonation products during the explosion. This effect is known as the "Munroe effect" [1].
If this cavity is lined with a material- for example: copper, magnesium, ceramic- then this material shall be projected into a "jet" [1]. This jet's velocity is correlated with both the geometry and choice of energetic used in the charge. This effect is exploited in several fields, which shall be explored in section 2.2.
It should be noted that the jet does not melt during this process, and instead exists as a solid material, undergoing extreme plastic deformation. Therefore, ductile materials, such as copper, are commonly used. The jet does not "melt" through targets, it instead erodes through due to the large amount of energy present. Both theories are likely linked to the acronym "HEAT", which describes a high explosive, anti-tank shaped charge warhead used by the United States, however this is simply an acronym, and does not describe the function of the warhead [2].

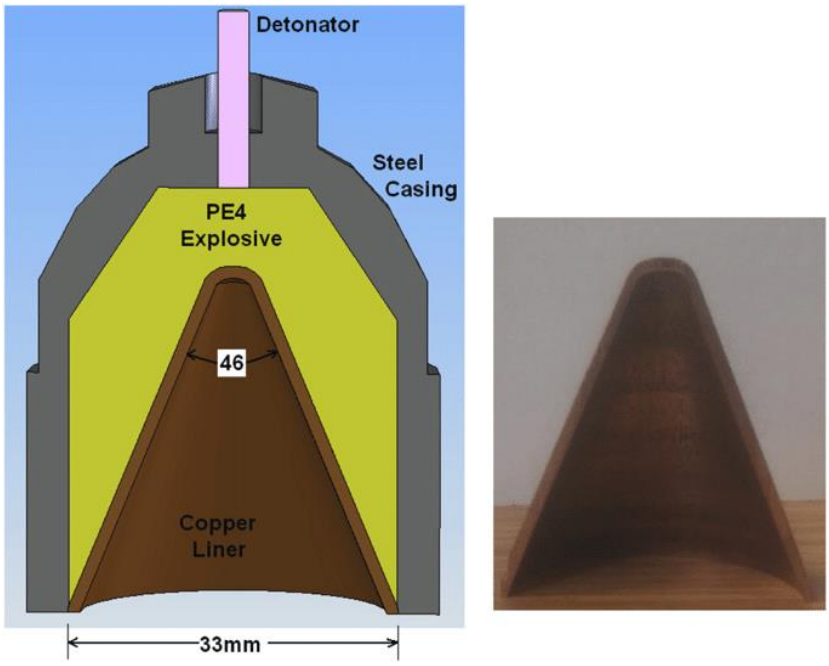

Figure 1 – An example of a shaped charge, with a copper liner [3].

2.2 Shaped Charge

2.2.1 Overview

The first concept of the shaped charge was seen in 1892, attributed to Franz von Baader, who explored the "hollow charge" with gunpower used as an energetic [4]. The first high explosive shaped charge was developed by G. Bloem, who patented detonating caps with hemispherical ends, which functioned in the same manner as a shaped charge, by focusing the power of the explosive using the Munroe effect, resulting in a more effective detonator [4]. These works were later rediscovered, and further developed by Charles Munroe, who proved explosive engraving using hollow charges, and showed that their use could increase target penetration [4]. Over the years, this concept has been developed into the technology seen below, with multiple uses and specialist charges.

2.2.2 Civilian Applications

Shaped charges are best suited to applications where an intense, localised force is required for the purposes of penetration [4]. Shaped charges are commonly used in oil and gas, where they are used to aid in the drilling of wells [5]. They are used in both cutting and fracking applications- the latter whereby multiple small, shaped charges are used to create fractures around wells, thus increasing the permeability of rock & increasing the flow to the well [5]. Figure 2 shows an example of the use of multiple shaped charged in an oil well fracking device, where a long rod with shaped charges within is lowered down into a well, and then utilised to create multiple small perforations into the rock walls of the well [6].

Figure 2 – HERO O-FRAC, an example of shaped charge uses in oil well fracking [6].

2.2.3 – Defence Applications

In terms of defence applications, shaped charges are generally used to penetrate through armour, for example, the HEAT round described earlier, is a shaped charge designed to penetrate through tank armour [2]. They are commonly used in multiple weapons systems including but not limited to handheld anti-tank systems, tandem warheads, air to ground weapons, air to air missiles, surface to air missiles & bunker busting bombs [4]. Figure 3 shows a HEAT round, where the conical copper shaped charge can be seen at the front of the round. The shaped charge penetrates the armour of the tank, and projects spall & detonation products into the tank, ideally resulting in the ignition of energetics within the tank.

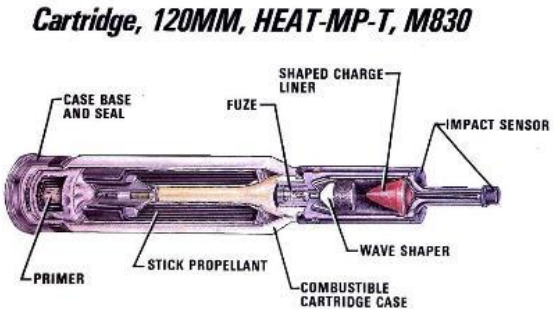

Figure 3 – M830 High Explosive Anti-Tank (HEAT) Cross sectional Diagram [7].

Shaped charges have also been developed into complex weapons technology to augment penetration of bunker busting bombs, an example of this is the AGM-154C Joint Standoff Weapon [8]. The system uses a tandem warhead, based on the BROACH concept, comprising of a shaped charge and a follow through bomb. The shaped charge is used to penetrate through hard targets, while the follow through bomb uses its kinetic energy to follow the penetration through till it is detonated. The result is greatly increased penetration when compared to that of a bomb relying on kinetic energy alone [8].

Figure 4 – Shaped charge and follow through bomb as used in AGM-154C [9].

As seen in the examples' above, shaped charges are primarily used to penetrate through armour, however they may also be used in explosive ordnance disposal (EOD) to initiate "low order" burning of unexploded ordnance (UXO), rather than conventional detonation which could be unfeasible in some circumstances. An example of this is Alford's Dioplex line of products, which uses a linear shaped charge to create cuts in UXO to allow energetic products to escape, rather than burning to detonation [10].

Figure 5 – Alfords Technologies Dioplex EOD (linear shaped charge) fitted onto UXO [10].

2.3 Shock Physics

2.3.1 - Introduction

Due to the complexity of the modelling to be undertaken, an understanding of shockwave physics is required to proceed. The formation & propagation of shockwaves directly effects the functionality of shaped charges. A high explosive is an explosive with the ability to detonate, which is to react at a rate faster than the speed of sound, where the material surrounding the detonating material is initiated via the pressure imparted by the shockwave moving through the material, not by thermal effects [11].

2.3.2 – Euler Equations

The Euler equations describe the conservation of mass, momentum and energy in flowing gasses. The conservation of mass is described as:

$$m = \frac{dm}{dt} = \rho A u$$

Equation 1 – Euler Conservation of mass across a normal shock [11].

Where m is the mass rate of flow, ρ is density and A the cross-sectional area. The flow through a normal shock with a frontward face of x and rearwards of y, both the mass flow rate and area of cross section remain unchanged as described below [11].

$$Mx = My \;\; and \;\; Ax = Ay$$

Equation 2 – Where mass flow rate and area remain constant [11].

The conservation of energy described that for a steady flow of a moving stream, without heat, work done or energy change, the principle describes that the sum of enthalpy and kinetic energy remains constant, as described in the equation below, where the Asterix represents a reference value [11].

$$C_p T + \frac{u^2}{2} = constant = C_p T^* + \frac{(a^*)^2}{2}$$

Equation 3 – Euler Conservation of Energy in a steady flow, where heat, work done and energy change are not considered [11].

The conservation of momentum described the forces acting on the upstream face of the shock, which are the sum of the pressure forces ($P_x A$), and those associated with the inertial effects of the wave (mu_x). The same is true for the downstream face. When a normal shock is in steady flow, these forces are in equilibrium [11]:

$$P_x A + mu_x = P_y A + mu_y$$

Equation 4 – Euler Conservation of Momentum, across a normal shock in steady flow [11].

2.3.3 – Rankine-Hugoniot Equations

The above equations may be rearranged to form the Rankine-Hugoniot equation which describes normal shock in ideal gasses [11].

$$\frac{k+1}{2k}(a^*)^2\left(\frac{1}{u_x} - \frac{1}{u_y}\right) = \frac{k+1}{2k}(u_y - u_x)$$

Equation 5 – Rankine-Hugoniot Equation, where u is velocity [11].

2.3.4 – Rayleigh Line Relationship

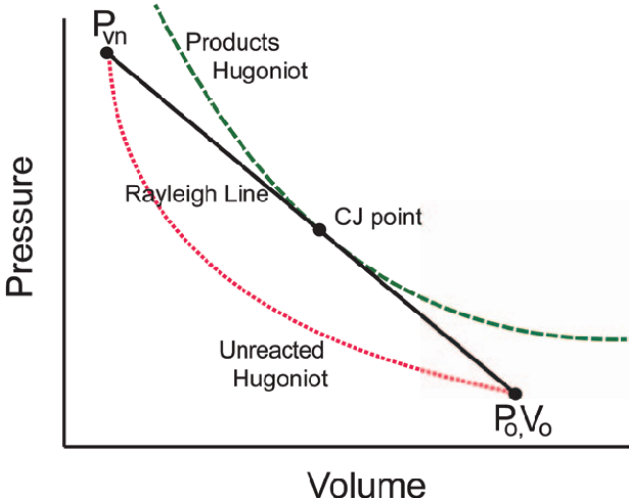

Figure 6 – Hugoniots and Rayleigh Line [12].

The Rayleigh line describes the relationship between unreacted and reacted Hugoniot lines in a shock front. Using this, we can consider an unreacted explosive's density or volume at a given pressure, measure the shock velocity and the particle velocity to find the reacted Hugoniot. This can then be used to find the unreacted Hugoniot [12]. These properties are then used to determine the Jones-Wilkins-Lee Equation of State parameters, which are used to model the behaviour of the shockwave traveling through the explosive.

2.3.5– Jones-Wilkins-Lee Equation of State

The Jones-Wilkins-Lee (JWL) Equation of state (EOS) is an equation specifically used to model the thermodynamic behaviour of explosives undergoing detonation [13]. Contrary to other EOS, the JWL equation can capture the rapid pressure expansion and decay which an explosive detonation causes [13]. This EOS shall be used to model the detonation of the explosive in the shaped charge to best accuracy during this study. The JWL EOS is below.

$$P = \lambda[Aexp\,(R_1\,V_r) + Bexp\,(-R_2\,V_r) + \,CV_r^{-(\omega+1)}$$

Equation 6 – Jones-Wilkins-Lee Equation of State

3 Modelling Scope

3.1 Overview

The aim of the study is to understand the impact of changing the cone angle on both the velocity and shape of the jet formed by a conical shaped charge. To do this, two charges shall be considered as described below. The modelling shall be undertaken using Abaqus explicit dynamic software, and results shall be validated using existing available studies, due to the lack of feasibility for physical trials to take place.

Both charges shall be filled with the same amount of explosive, with shall be "PE4" or "Plastic Explosive 4" also known as "C4", an RDX based plastic explosive, containing around 87% RDX and 13% binder, including a marking agent [14]. The high percentage of RDX results in a powerful blasting explosive, ideal for use in shaped charges. PE4 is used in "user filled" shaped charge systems across the world.

Due to the focus of the study, the model shall be developed to prioritize fine nodal elements, to ensure that the shape is as of higher accuracy as is feasible. The velocity shall be measured from the nodes nearest to the tip of the projected jet. With fine nodal elements, a fine mesh is required, which may require additional complex modelling techniques to prevent overstressing of individual mesh elements – which can be summarized as the elements being stretched, by the force of the explosive forming, beyond what is tangibly feasible to model with accuracy.

These techniques include: The usage of sculpted meshing – to prioritise critical areas, adaptive meshing – which redevelops the mesh between simulation increments, to prevent elements from becoming over stretched – and solid particle hydrodynamics, which can be applied where elements are about to become over stretched, and makes the element behave as a flowing particle which cannot deform, rather than a section of a solid material.

These techniques are complex and can result in the loss of accuracy in differing ways. For example, solid particle hydrodynamics allows particles to flow more freely than they may in a solid meshed part, resulting in an increased velocity. They may also disobey laws of symmetry in the model, as the particles are entirely unconstrained, and shall only respond to the forces applied to them, excluding the fixtures within the modelling. Other limitations shall be described in more detail during modelling.

3.2 Charge A

Charge A is a conical shaped charge with a cone angle of 60°, based upon a shaped charge from a similar study [15]. A technical drawing of the charge is available in appendix A. In theory, this charge shall produce a jet with a fine tip, travelling at 6.3 km/s [15]. Due to the similarities with the other study, this charge shall provide validation for both jet velocity & geometry. This study shall use PE4 as opposed to the TNT fill used in the other study [15]. Dimensions for this charge are available in appendix B.

3.3 Charge B

Charge B is a variation of Charge A, where it is identical apart from the angle of the conical liner being changed to 70°. Dimensions are available in appendix B.

4 Literature Review

4.1 Shaped Charge Modelling

4.1.1 – Introduction & Scope

Prior to undertaking modelling, it is critical to understand the factors which may influence the results and to consider how validation may take place. This shall focus on the primary factors identified via an initial literature review, those being: Geometry, Energetics, Materials & Scope of modelling. It shall also consider methodologies for use in result validation.

4.1.2 – Geometry & Materials

4.1.2.1 – Geometry

The most referenced effector of the liner geometry is the apex angle, in conical shaped charges. Generally, the larger the angle of the cone, the lower the velocity of the tip of the jet and vice versa [16]. The thickness of the liner effects the velocity of the jet formation, with thinner liners losing less velocity over time when compared with thicker liners, until a middle point is reached, after which the inverse effect can be seen [17]. This shows that the liner thickness must be balanced for peak efficiency.
The detonation point is the point at which the energetic is initiated, this location of this in the charge is critical for the effective exploit of the Munroe effect [18]. The "head-height" is the distance between the tip of the charge liner and the point at which detonation is initiated, this is a key dimension, as it affects the shape of the detonation wave. If the detonation wave has not yet fully formed, it is likely to be a spherical shape, which shall result in a non-uniform collapse of the liner, reducing the effectiveness of the charge [19].

4.1.2.2 – Energetics

The energetic used in the charge will directly affect the jet velocity. The velocity of detonation of different energetics varies, which will directly impact the peak velocity which a jet may reach, and the total amount of energy imparted.

4.1.2.3 – Materials & Scope of Modelling

In this simulation, all materials are treated as "perfect", where they do not have imperfections in their structure – which could include bonding structures, cavitation & impurities. This means that modelled results will likely never reflect that of a real-world shaped charge but may provide a close match. It is critical that this is understood throughout.

4.1.3 – Validation of Jet Velocity

To validate the jet velocity, different techniques may be used depending on the precision required.
The Gurney Equations are primarily used to predict the velocity of fragmentation and flyer plates; however, they may also be used with shaped charges [20]. The results of this method are of low accuracy, as they assume that detonation product expand uniformly with constant density and shockwave effects are neglected [20].
The Pugh-Eichelberger-Rostoker model may also be used, which is more specialised for use in shaped charges, it considers the geometry of the charge in addition to the factors included by the Gurney Equations [21].

5. Modelling Setup

5.1 Material Properties

In this study, the shaped charge cone shall be considered as an oxygen free copper, as this material is often used in real products. It also has few impurities in the real world, which shall make the modelling more effective, as it does not consider impurities or differing structures. The material properties were sourced from another study [22].

The casing is less critical, as it shall be destroyed during the detonation, and in the context of this study, it shall not be used in the results, excluding the validation of the detonation shockwave. It is specified as 6061-T6 aluminium [23].

The explosive fill is critical to performance, where typically a high velocity of detonation is preferred, to impart the maximum velocity into the shaped charge jet, through maximum metal acceleration. A high explosive is required, in this study plastic explosive 4 (PE4, or C4) is considered, due to its high RDX content (87% [14]), and usage in several existing products. In terms of the required parameters, the Jones-Wilkins-Lee (JWL) model is used, to predict the expansion of detonation products during reaction. These are included in figure 7 below.

JWL EOS – PE4								
ρ_0 ($\frac{g}{cm^3}$)	A (GPa)	B (MPa)	R1	R2	ω	E0	D (m/s)	Pcj (GPa)
1.495	1800	10.153	6.271	1.05	0.2	6596	7550	21.42

Figure 7 – JWL EOS Parameters for PE4 [24].

5.2 Meshing

Meshing is the process of breaking down CAD geometry into a mesh of individual nodes, which are used to calculate interactions. CAE requires the use of nodes, due to the limitations of computing- where each node shall require a calculation, an infinite number of nodes would require an infinite amount of time [25]. Thus, meshing is designed to find a balance between the precision of the study & the computational power required to run it. In this study, the casing is only required to provide a somewhat realistic simulation of the confinement of detonation products, and as such is left with a coarse mesh. The explosive charge requires finer detail towards the cavity liner, where the most interaction shall occur- as such it is dynamically meshed, with coarser nodal points where less detail is required and vice-versa. The same approach is adopted in the implementation of the liner mesh, where the outer edges are of less interest. The result is the mesh seen in figure 8 below, further detail on the method used to implement this mesh is included in section 6.

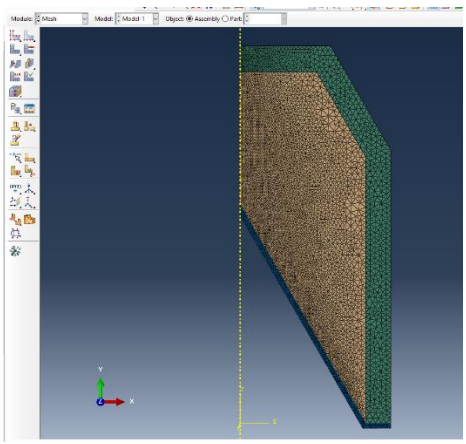

Figure 8 – Example of a meshed shaped charge.

Due to the nature of the high energies imparted during this study, it is expected that nodal elements shall fail because of excess distortion (where they are stressed beyond their computable limit). To reduce these errors, two techniques may be implemented- adaptive meshing & solid particle hydrodynamics. Adaptive meshing is the process of automated re-meshing between simulation steps, to prevent elements from becoming excessively distorted. Essentially, the selected body shall be re-meshed at a set number of steps. This may affect the accuracy of the simulation but allows it to run long enough to provide meaningful results.
Solid particle hydrodynamics (SPH) converts the meshed elements into a solid particle once a set criterion is reached, which could be time or stress based, and effect all or individual nodes. This again reduces the impact of overstressed elements, however it may result in a larger increase in simulation error, as the particles shall act as dimensionally free, rather than constrained to one another through material bond. Symmetrical boundary constraints are also lost with this method.
It is planned to experiment with both methods; however, it is expected that SPH shall greatly reduce accuracy and thus shall not be used in the main results unless required.

5.3 Interactions & Fixtures

Interactions describe the interactions between different bodies in the simulation, these must be defined as without them, the simulation shall not consider the effect of the detonation products on the liner or casing. In terms of this simulation, all bodies may interact with one another.
A fixture is used to define an attachment, or a line of symmetry in a model. In both two- & three-dimensional models, the fixture is used to define symmetry, due to the half geometries used, to ensure that results are not affected. This is accomplished by defining a symmetrical fixture along the applicable axis on the model. This shall be detailed in section six.

5.4 Limitations

Due to the reality of computational modelling, some limitations apply. Structural & material impurities are not considered in this study, however materials where few are likely to exist have been specified where this is critical to reduce the impact that this limitation has.
To reduce the complexity of the models, half sections are used with symmetrical fixtures, to reduce the overall number of nodes required. In some cases, the symmetrical fixtures fail to constrain the jet of the shaped charge, resulting in a potentially reduced velocity.
The jet shall have no resistance once projected, as either air, or a target is not included in the scope of this modelling.
Time & computational constraints limit the fineness of the meshing of bodies, resulting in the potential for unrealistic deformation, especially in complex geometries. This has been limited using structured meshing, where possible.

6 Setup

6.2 General Setup

6.1.1 – Material Properties

Material properties, as detailed in section five, are loaded into the Abaqus software, and defined into the required bodies as detailed in figure 9 below. These are defined as solid, homogeneous bodies, with no impurities or variation. Once inputted into Abaqus, they are assigned to the relevant sections within the assembly. Evidence of this input into Abaqus is included in appendix A.

Material Properties				
Material	**Body**	**Source**	**Parameters**	
PE4	*Charge*	[14]	*JWL Equation of State*	
			ρ_0	1.495 g/cm^3
			A	1800 GPa
			B	10.153 GPa
			R1	6.271
			R2	1.05
			ω	0.2
			E0	6596
			D	7550
			Pcj	21.42
Oxygen Free Copper	*Liner*	[22]	*Johnson-Cook Parameters*	
			A	90 MPa
			B	292 MPa
			C	0.025
			m	0.31
			n	1.09
			Density & Elasticity	
			Density	8960 kg/m³
			Youngs Modulus	110 GPa
			Poison's Ratio	0.343
6061-T6 Aluminium	*Casing*	[23]	*Johnson-Cook Parameters*	
			A	324.1 MPa
			B	113.8 MPa
			C	0.002
			m	1.34
			n	0.42
			D1	-0.77
			D2	1.45
			D3	-0.47
			D4	0.0
			D5	1.6
			Density & Elasticity	
			Density	2700 kg/m³
			Youngs Modulus	69 GPa
			Poisson's Ratio	0.33

Figure 9 – Material properties, as used in simulation.

6.1.2 – Interactions

Some simplifications are made in this area, due to the limitations of the scope of study. Tangential behaviour is defined as frictionless, to reduce the computational burden of the simulation. The normal behaviour is defined as "Hard" contact, meaning that materials shall not pass through one another, which is not realistic, but again reduces computational burden. Details of the setting of these interactions may be found in appendix C.

6.1.3 – Mesh Type & Control

For all models, the mesh shape is defined as trimetric, due to the shape of the cone liner. This is defined in the mesh step, under mesh controls. Free meshing is defined, as structured meshing shall be controlled via nodal seeding in the individual meshing steps. This is defined in figures 10 & 11 below.

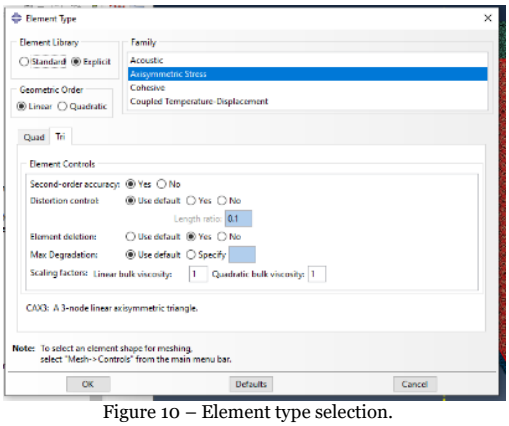

Figure 10 – Element type selection.

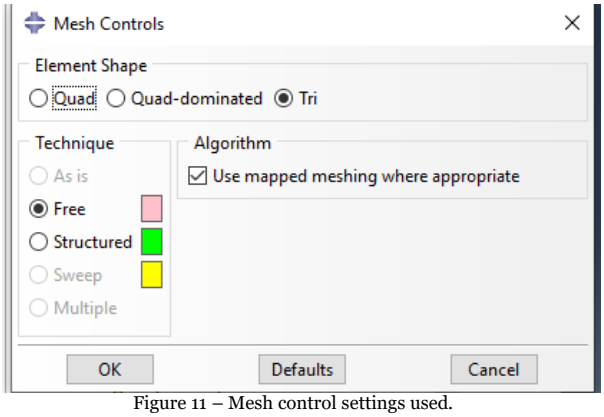

Figure 11 – Mesh control settings used.

6.3 Charge 1 – 2D

6.2.1 – Parts, Properties & Assembly

The bodies are draw in two dimensions and specified as two dimensional bodies for a simplistic simulation. Each body is drawn according to the dimensions taken from the comparative study [15]. Dimensional drawings are available in appendix B. Once drawn, these are defined as solid 2-dimensional bodies.

These bodies are then assembled as they shall be used, with the casing around the outside of the charge, and the liner within the cavity. Colours are used to show the different materials in the assembly in figure 12.

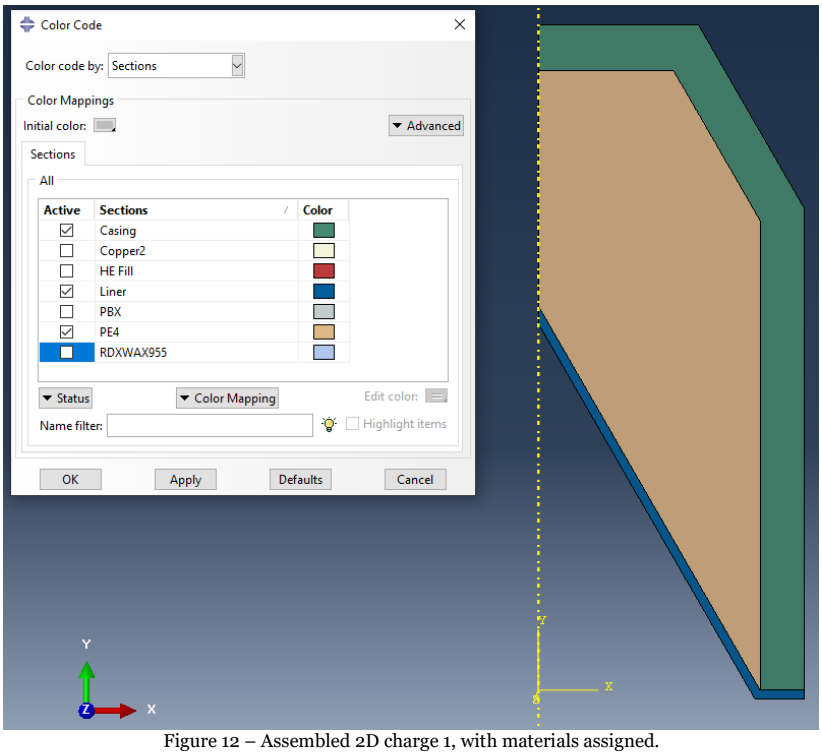

Figure 12 – Assembled 2D charge 1, with materials assigned.

6.2.2 – Meshing

As discussed in section five, structured meshing is used to prioritize the areas of most interest. The liner is meshed with a gradient between incredibly fine mesh at the tip to a coarser mesh at the end near the liner. The challenge here could be that these fine elements at the tip of the cone become over distorted, so additional techniques may be required. The filling contains a reasonably linear mesh, however some structuring is used to add coarser elements in areas such as the outer edges away from the cone, where they shall have little impact on the cone. The casing does not use structured meshing, instead containing a linear mesh due to the limited interest in this body. Figure 13 shows the fine liner mesh with gradient applied & figure 14 shows the whole model.

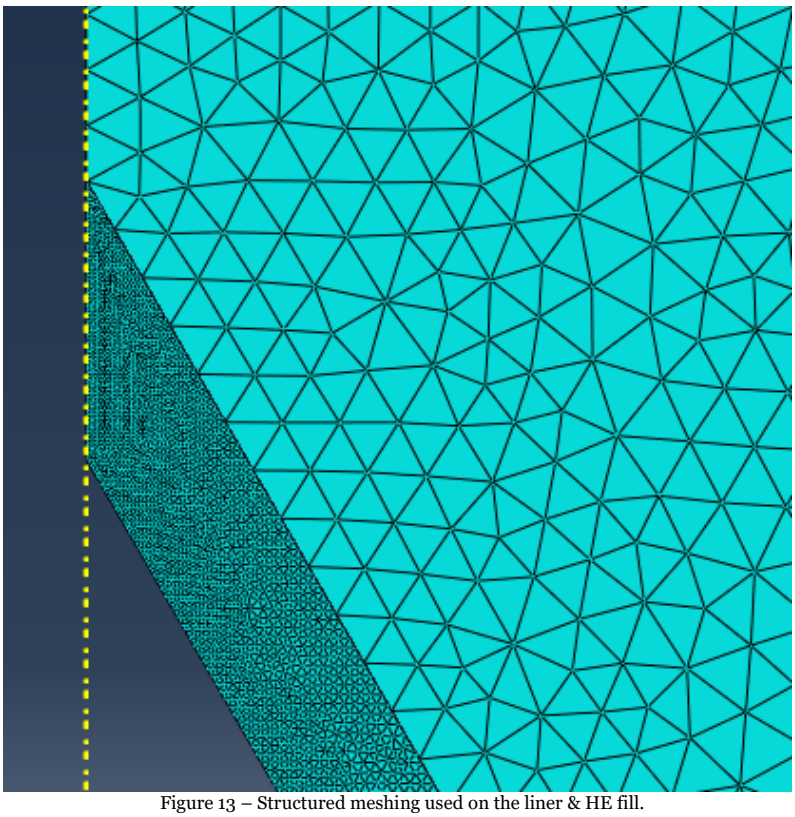

Figure 13 – Structured meshing used on the liner & HE fill.

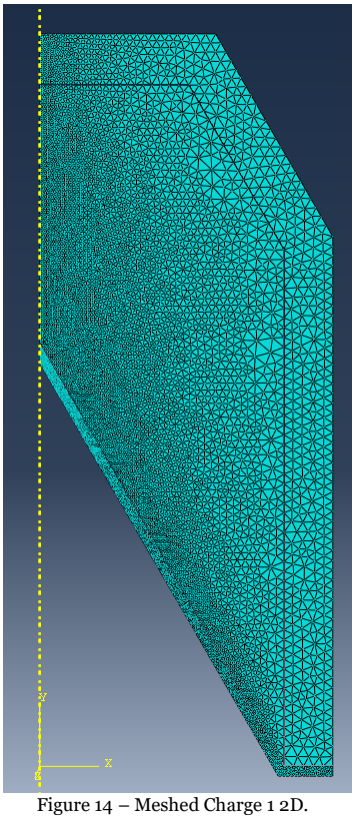

Figure 14 – Meshed Charge 1 2D.

6.4 Charge 2 – 2D

6.4.1 – Parts, Properties & Assembly

Details are drawn as used in charge 1, except for the change of cone apex angle, which is increased to 70*. The thickness of the liner is also marginally increased, with the intention of reducing the element distortion errors seen during the simulation of the first charge. The assembly mirrors that of charge 1. Dimensional drawings are available in appendix B.

6.4.2 – Meshing

The same meshing strategy was used to implement a mesh on charge 2, with a decrease in the number of nodes in the casing and outer edges of the HE fill due to the lack of interest in this area. The final mesh is detailed in figure 15.

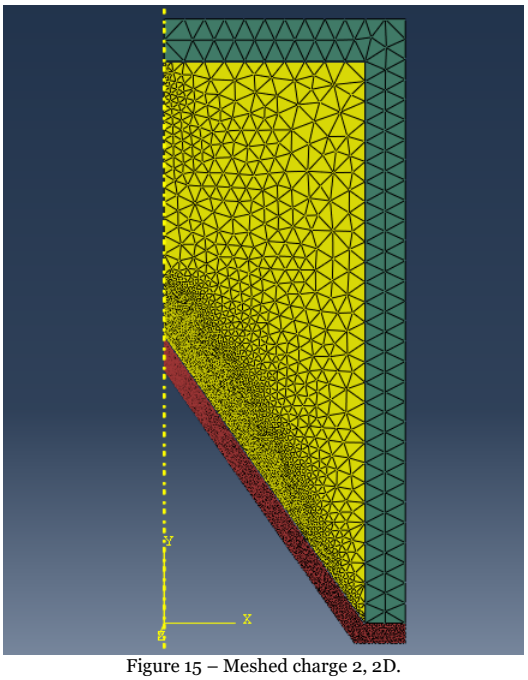

Figure 15 – Meshed charge 2, 2D.

6.5 Charge 2 - 3D

6.5.1 – Parts, Properties & Assembly

The 3-dimensional charge 2 is based upon the same dimensions as charge 2 but revolved around 180 degrees. The charge was not revolved a full 360 degrees to reduce the total number of nodes in the simulation, and instead a symmetry constraint was used to replicate this. Figures 16 – 17 show the 3-dimensional components. They are assembled as previously. All dimensions are available in appendix B.

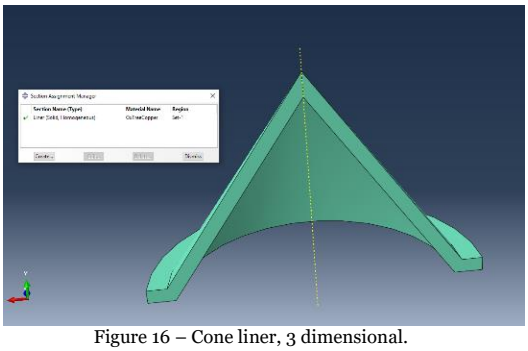

Figure 16 – Cone liner, 3 dimensional.

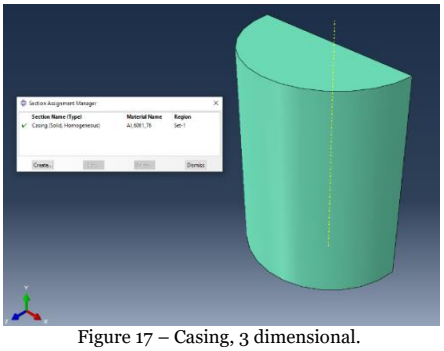

Figure 17 – Casing, 3 dimensional.

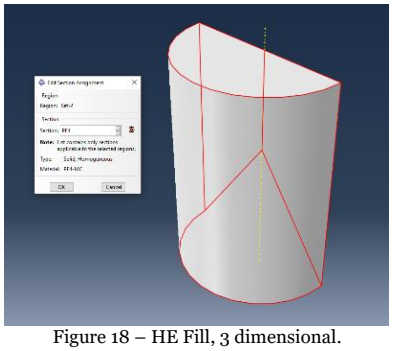

Figure 18 – HE Fill, 3 dimensional.

6.5.2 – Meshing

Due to Abaqus licence limitations, the number of nodes must be used as efficiently as possible to minimise computational load & total number. The same strategy as charge 2 was employed, with a finer mesh used in areas of interest, with a gradient to the coarser mesh. The completed mesh is shown below in figure 19.

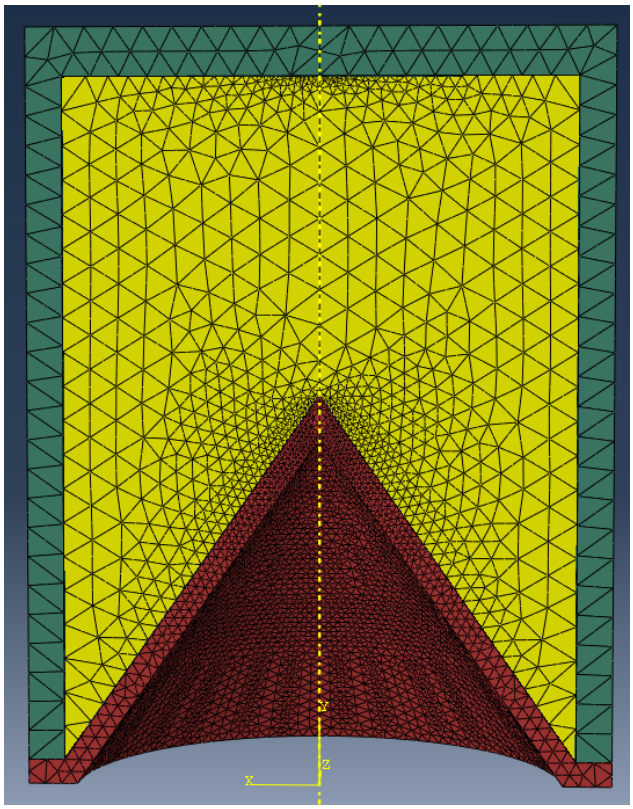

Figure 19 – Meshed charge 2 – 3D.

7. Results

7.1 Charge 1 – 2D

After several iterations of meshing, to reduce challenges associated with excess element distortion, a running simulation was reached. The strategy used implemented adaptive re-meshing, alongside structured meshing to reduce the number of errors seen. The simulation ran to a suitable time, at which point the charge liner had produced a jet, but had not fully inverted. A peak velocity was seen which was within a reasonable error margin of the expectation, especially considering the lack of cone inversion. It was not feasible to run the simulation for any longer, due to the challenges of excess distortion in the tip of the jet, even with the implementation of the methods to combat this.
The detonation front in the charge did not travel as expected the pressure map in figure 20 show the initial detonation taking place at the tip of the cone, rather than the top of the charge. This is due to a modelling error, however the jet still propagated, just at a lower velocity than expected, and with a non-uniform liner collapse, resulting in the excess distortion failures seen. To prevent errors in the further models, a short simulation was run & pressure maps confirmed to ensure detonation taking place from the proper point.

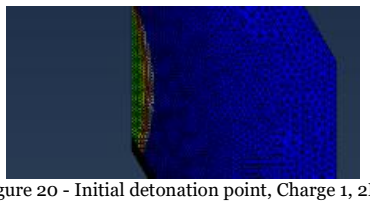

Figure 20 - Initial detonation point, Charge 1, 2D.

In terms of the shape of the jet, the charge produced an incredibly fine tipped jet, which is due to the angle of the cone combined with the uneven liner collapse resultant of the improper initiation. In comparison to the verification study, the tip of the jet is significantly finer than expected, again likely related to the improper detonation point & potentially the lack of formation of the total jet. In the other simulations, it is hoped to form a more total jet to provide a more accurate comparison.

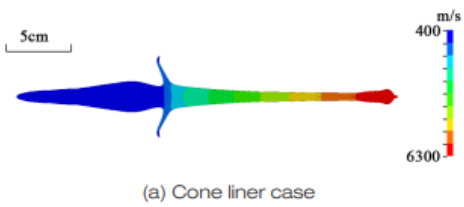

Figure 21 – Comparative jet [15].

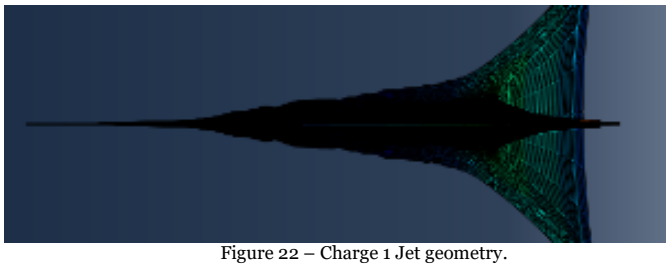

Figure 22 – Charge 1 Jet geometry.

The velocity of the jet reached a peak of circa 5.5 km/s, which is lower than anticipated, but likely due in part to the incorrect starting location for the detonation, which may have prevented the peak velocity of detonation from being reached before imparting force on the liner in addition to a non-linear application of force onto the liner. Remeshing of elements may also impact the velocities, SPH may offer a more accurate representation of velocity in the jet. Full results from Charge 1 2D are available in appendix D.

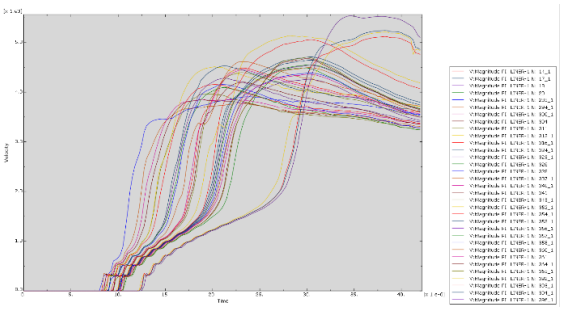

Figure 23 – Velocity, tip of jet, charge 1, 2D.

7.2 Charge 2 – 2D

The same strategy, adaptive re-meshing & structured meshing, was used to produce a long running simulation for the second charge, however the differing geometry resulted in a more linear acceleration of the charge liner, the simulation ran till the cone had inverted, and a long jet formed, providing a more realistic output.

It should be noted that the detonation point error was corrected, and the detonation did take place at the rear of the charge, as seen in figures 24 & 25 below.

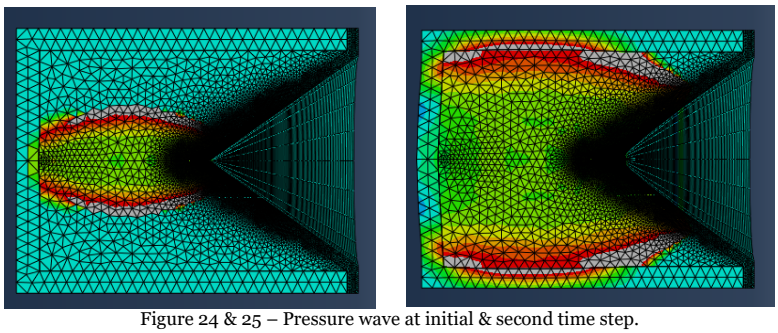

Figure 24 & 25 – Pressure wave at initial & second time step.

The jet's velocity provided the desired result, reaching a peak of 7 km / s. This is inverse to the expectation that increasing the cone angle results in a reduced jet velocity. This is likely linked to the better formation of this model when compared to charge 1.

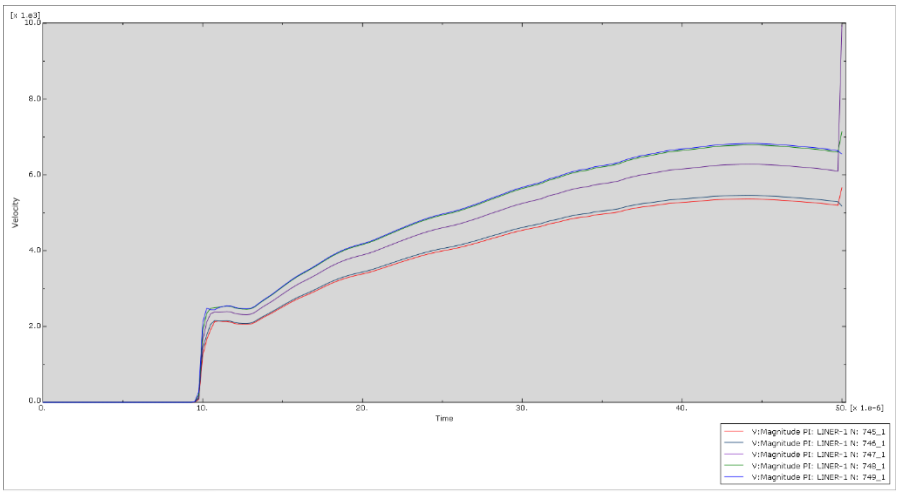

Figure 26 – Charge 2, 2D Jet Velocity plot.

The jet's geometry is very fine, which would likely result in an unstable jet which may breakdown in atmosphere, and as such loose its effectiveness. Below is a comparison between the geometries produced between charge 1 & charge 2. The primary difference is the size of the slug (mass area formed where the cone collapses) being significantly shorter and thicker in charge 2's jet. This is a result of the change in angle, allowing more of the cone to collapse into itself. If the simulation were to have run for longer, it would've likely produced fine, round tipped jet, followed by a large slug almost of EFP proportion. A full suite of results may be found in appendix E.

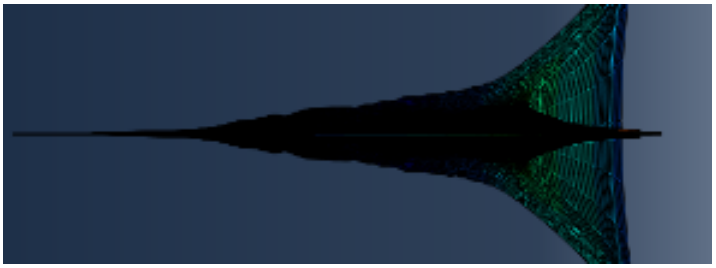

Figure 27 – Jet Geometry, Charge 1 2D.

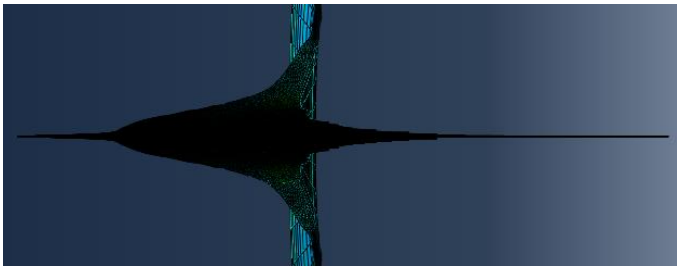

Figure 28 – Jet Geometry, Charge 2 2D.

7.3 Charge 2 - 3D

Based upon the success of the 2-dimensional study, a 3-dimensional study of charge 2 was conducted to provide more accurate results. Initially, challenges with excess distortion errors prevented the simulation from running to reasonable time step. To combat this, SPH was used to reduce the likelihood of particles failing. Initially, SPH modelling provided better running, however challenges were identified in bounding particles, which were no longer constrained by symmetry due to their properties, and as a result SPH modelling was abandoned.

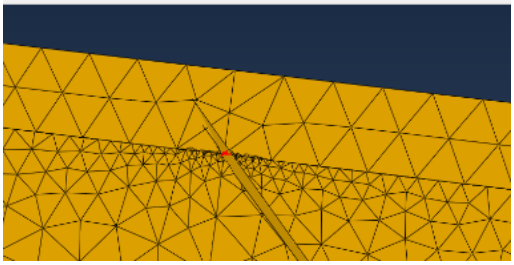

Figure 29 – Excess distortion error, highlighted red.

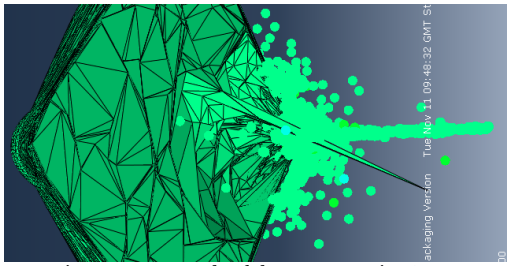

Figure 30 – Example of charge 2, 3D using SPH.

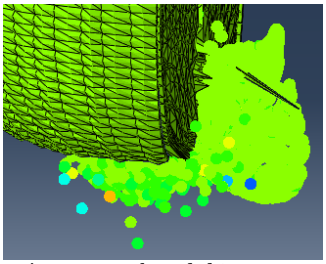

Figure 31 – Unbounded SPH error.

A more aggressive re-meshing strategy was implemented, resulting in more effective running of the simulation, running to a point further than was previously possible in 2-dimensional modelling. The jet produced is much more like that of the reference study, however, the rounding to the tip of the jet is still not seen. This may be due to the lack of air / target resistance, resulting in the jet experiencing no resistance in formation- explaining this lack of distortion. The rear of the slug is also finer than anticipated. However, the overall shape is more accurate than previously seen.

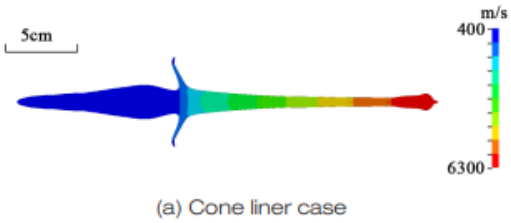

Figure 32 – Comparative Jet [15].

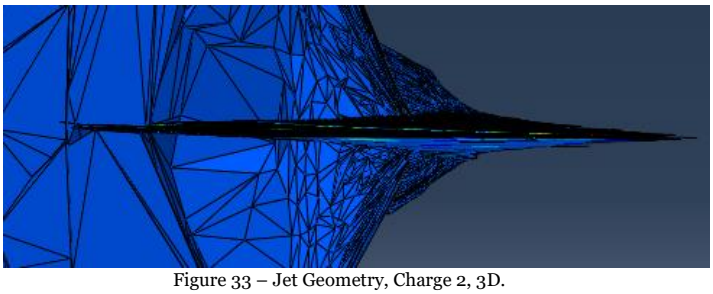

Figure 33 – Jet Geometry, Charge 2, 3D.

The velocity was significantly lower than anticipated, with a peak of circa 3.5 km/s. It isn't obvious why this is reduced when compared with the 2-dimensional model but may be due to the 3-dimensional formation of the detonation wave's interaction with the liner, which may differ compared to that of the 2-dimensional model. The velocity is shown below in figure 31 & a full results set is available in appendix F.

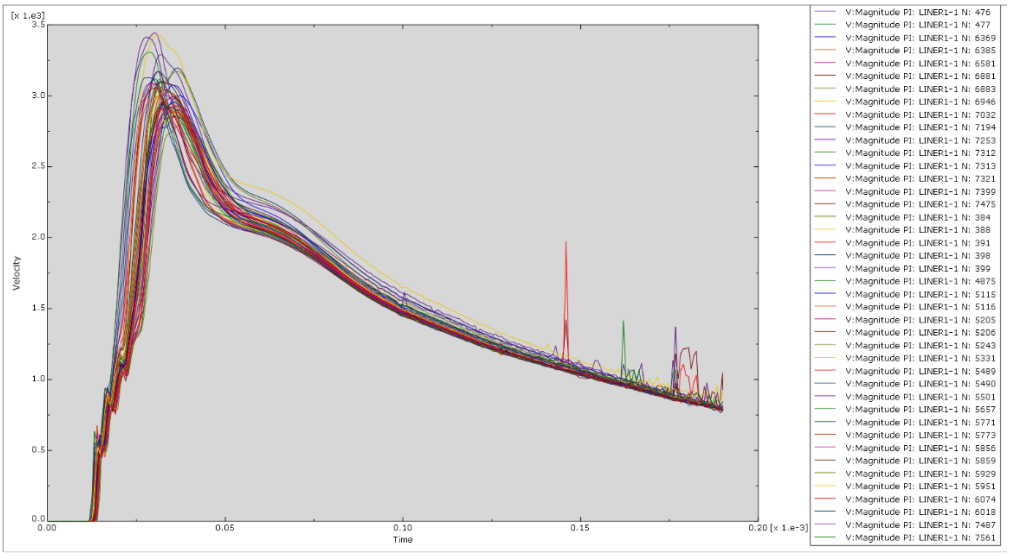

Figure 34 – Jet Velocity, Charge 2, 3D.

8. Validation

Validation of jet geometries was undertaken as part of section 6.1, the results were not entirely comparable to those seen in the comparable study, but this is likely due to the lack of running time in these simulations, combined with the lack of resistance to the jet (air / target). However, the rest of the jet's geometry is very similar to the comparative study, providing good confidence excluding the tip of the jet.

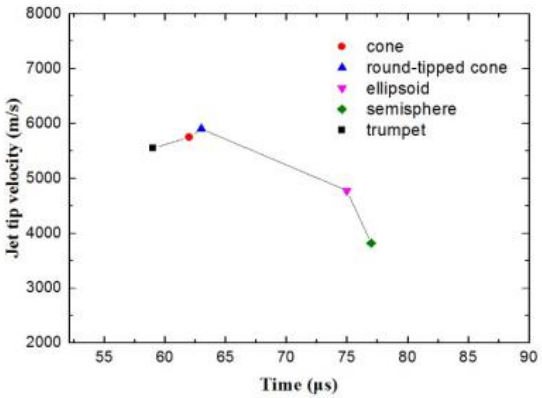

Figure 35 – Jet tip velocity, comparative study [15].

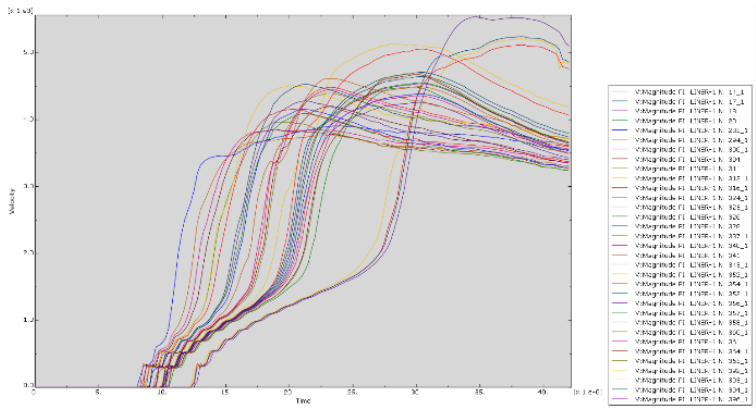

Figure 36 – Charge 1, 2D, Jet tip velocities.

In terms of the velocity of the jet, the results seen are very similar. It should be noted that the comparable study uses a TNT HE fill, which may produce a different velocity. Peak velocity is slightly reduced, but accurate within 1 km/s as seen above, considering the differing HE fills, there is a reasonable confidence in the velocity produced. It should also be noted that the detonation was not initiated in the correct position, which may have resulted in the slightly reduced velocity.

Overall, the model provides good confidence in the jet velocity & geometry, excluding the tip of the jet, which shall not be considered as accurate. If the model were to be used for precision work, more comparative studies may be used to provide a higher level of confidence in the model.

9. Conclusion

In conclusion, the model has produced a reasonably accurate jet geometry, however the velocity is not comparable to existing models or between 2-dimensional & 3-dimensional, and as such should be treated as invalid. This may be related to the small head height of the charge, which does not allow the detonation shockwave to fully form before imparting force upon the liner, resulting in erroneous results. The results of charge 1 are invalid, as the point of detonation was incorrect, and as such the detonation wave would not meet the liner as expected.

The results give light to several improvements which could be made to the charge. During shockwave propagation, a large amount of material in the upper edges of the charge is not consumed until after the wave has passed, due to the shape of formation of the shockwave. As such, this material could be emitted from the charge, resulting in a more efficient use of explosives throughout.

Modelling such as this has also given light to the use of wave forming within the charge, to result in a more effective transformation of energy from the explosive into propulsion of the liner. This could be considered in future studies.

10. References

[1] W. P. Walters, “The Shaped Charge Concept, Part I Introduction,” US Army Ballistic Research Laboratory , 08 1990. [Online]. Available: https://apps.dtic.mil/sti/pdfs/ADA226401.pdf. [Accessed 01 10 2025].

[2] J. J. Milinazzo, “Energy Transfer of A Shaped Charge,” Sandia National Laboratories, 11 2016. [Online]. Available: https://www.osti.gov/servlets/purl/1334941. [Accessed 01 10 2025].

[3] T. Elshenawy, “Influences of target strength and confinement on the penetration depth of an oil well perforator,” Research Gate, [Online]. Available: https://www.researchgate.net/figure/The-shaped-charge-used-in-the-concrete-strength-study-left-and-a-cross-section-of-the_fig1_271574612. [Accessed 2025 10 2025].

[4] W. Walters, “A Brief History of Shaped Charges,” *Army Research Laboratory,* pp. 6-16, 2008.

[5] L. Albert, N. Nerry, H. Prapoo, P.Dai, B. Qu, G. Jiang and D. Kwok, “Integrating Propellant and Shaped Charges to Improve Frac Efficiency,” OnePetro, 05 09 2018. [Online]. Available: https://onepetro.org/SPELRBC/proceedings-abstract/18LRBC/2-18LRBC/D022S010R003/236681. [Accessed 13 10 2025].

[6] O. O. Tools, Artist, *HERO O-FRAC.* [Art]. CORE Laboratories, 2025.

[7] M. A. Network, Artist, *Cartridge, 120mm, HEAT-MP-T, M830.* [Art]. 1994.

[8] “AGM-154 Joint Standoff Weapon,” US NAVY Naval Air Systems Command, 27 09 2021. [Online]. Available: https://www.navy.mil/Resources/Fact-Files/Display-FactFiles/Article/2166748/agm-154-joint-standoff-weapon-jsow. [Accessed 13 10 2025].

[9] T. M. E. Ltd, Artist, *MAFIS(FSU-26/B) in JSOW (AGM-154C).* [Art]. 2000.

[10] Alfords Technologies, “Products, Dioplex EOD,” Alfords Technologies, 01 01 2025. [Online]. Available: https://www.explosives.net/products/dioplex-eod/. [Accessed 30 12 2025].

[11] G. F. Kinney and K. J. Graham, “Explosive Shocks In Air, Second Edition,” Springer Science+Buisness Media LLC, California, 11985.

[12] A. Minchinton, “On the Influence of Fundamental Detonics on Blasting Practice,” Research Gate, Sydney, 2015.

[13] ITASCA, “ITASCA Software Guide,” ITASCA, 27 10 2025. [Online]. Available: https://docs.itascacg.com/itasca940/common/models/jwl/doc/modeljwl.html. [Accessed 16 11 2025].

[14] H. Bornstein, V. Kuznetsov, J.-P. Lu, S. Stojko and J. Freundt, “Characterisation and validation of the JWL equation of state parameters for PE4,” International Journal of Impact Engineering, Edinburgh, 2022.

[15] Z. Liu, J. Zhai and S. Su, “Numerical Simulation on Conical Shaped Charge with Copper Liner in Several Typical Shapes,” *International Journal of Multiphysics,* vol. 13, no. 3, pp. 231 - 240, 2019.

[16] M. Shuai, “Simulation Study on Adjustable Structural Shaped Charge Water Jet forming and Penetrating Improvised Explosive Devices,” in *247th ESC Meeting*, Montreal, 2024.

[17] T. Elshenawy, E. Ezzat, A. M. Riad and M. A. Elkader, “Influence of Liner wall thickness on the penetration performance of PETN-HTPB PBX-based Shaped Charges into Steel Targets,” *Central European Journal of Energetic Materials,* vol. 19, no. 1, p. 78, 2022.

[18] I. G. Aksoy and S. Sen, “Effect of variation of conical liner apex angle and explosive ignition point on shaped charge jet formation.,” *Indian Journal of Engineering & Material Sciences,* vol. 10, no. 1, pp. 1-9, 2003.

[19] A. Gustafsson, “Shaped Charge Design - Construction of a miniaturized shaped charge,” Karlstads University, Karlstad, 2021.

[20] T. A. E. Elshenawy, “Criteria of Design Improvement of Shaped Charges Used as Oil Well Perforators,” The University of Manchester (UK), Manchester, 2012.

[21] K. Jiang, S.-C. Deng and H.-B. Li, “Theoretical Calculation and Analysis of the velocity of shaped charge jet with modified collapse velocity model,” University of Chinese Academy of Sciences, Wuhan, 2024.

[22] M. Olsson, H. Persson, M. Agmell, V. Bushlya and J.-E. Stahl, “FE simulation and experimental verification of side-flow and burr formation in,” Elsevier, Lund, 2018.

[23] D. G. Spear, A. N. Palazotto and R. A. Kemnitz, “Modeling and Simulation Techniques Used in High Strain Rate,” MDPI, Dayton, 2021.

[24] H. Bornstein, V. Kuznetsov, J.-P. Lu, S. Stojko and J. Freundt, “Characterisation and validation of the JWL equation of state parameters,” *International Journal of Impact Engineering,* vol. 164, no. 1, pp. 1-14, 2022.

[25] D. Madier, “An introduction to the fundamentals of mesh generation in finite element analysis,” FEA Academy, None, 2023.

11. Appendices

Appendix A – Interaction Setup

A-1 – Oxygen Free Copper

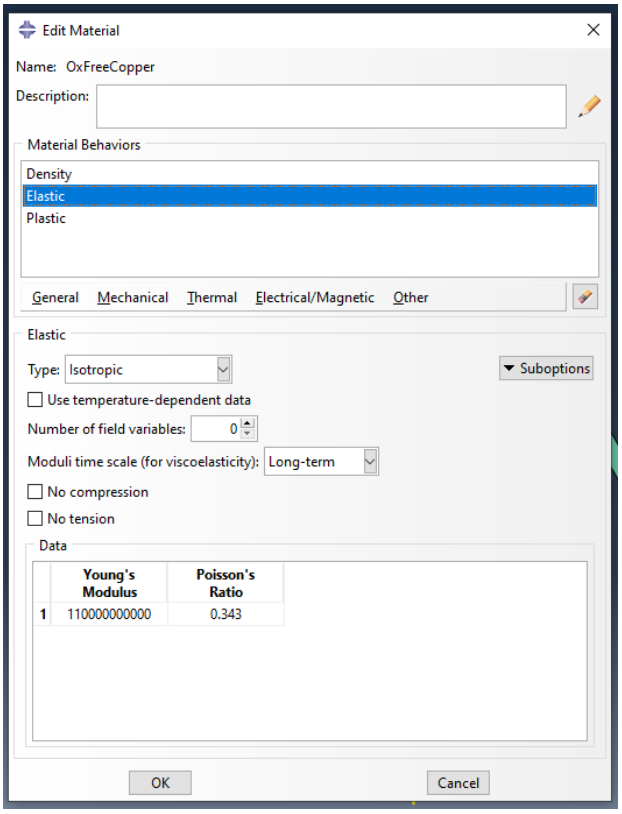

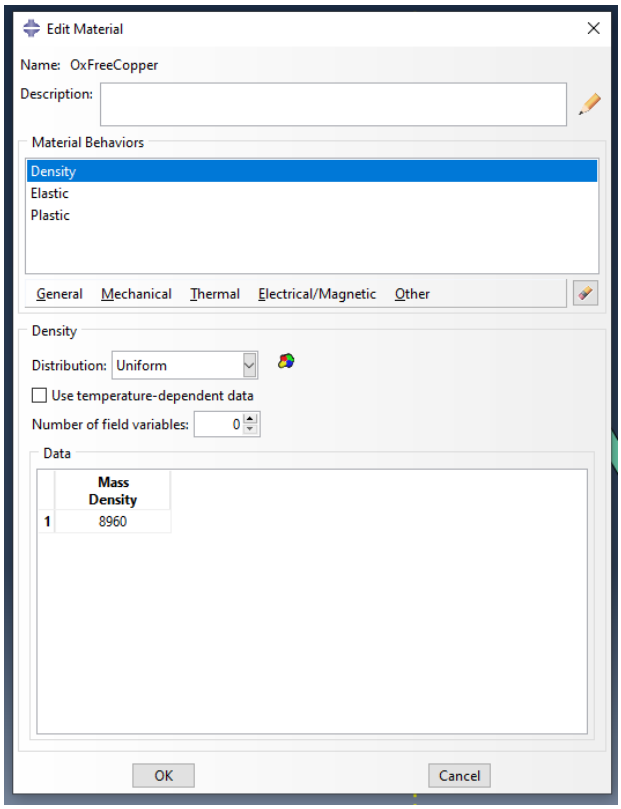

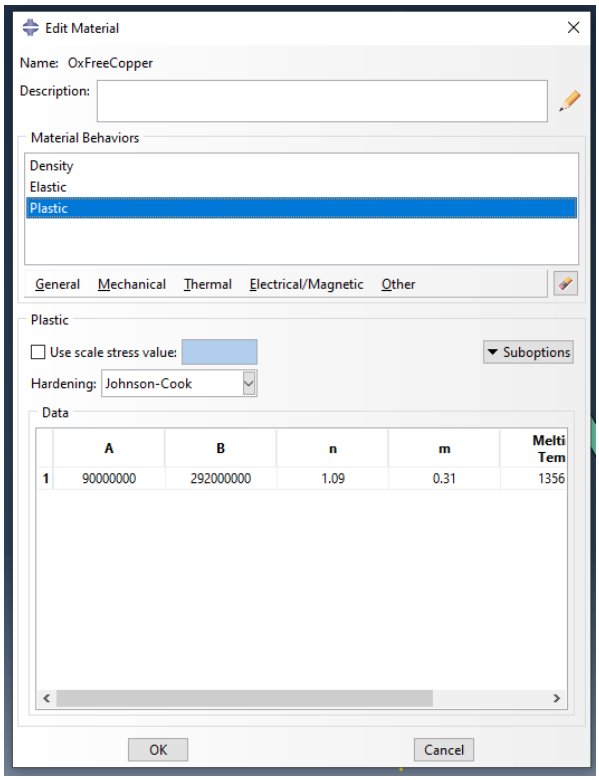

A-2– Aluminium 6061—T6

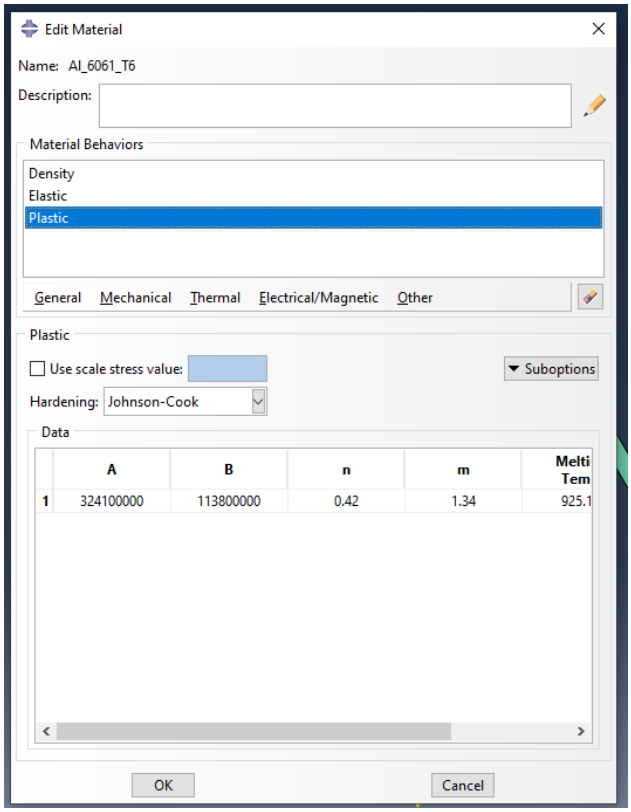

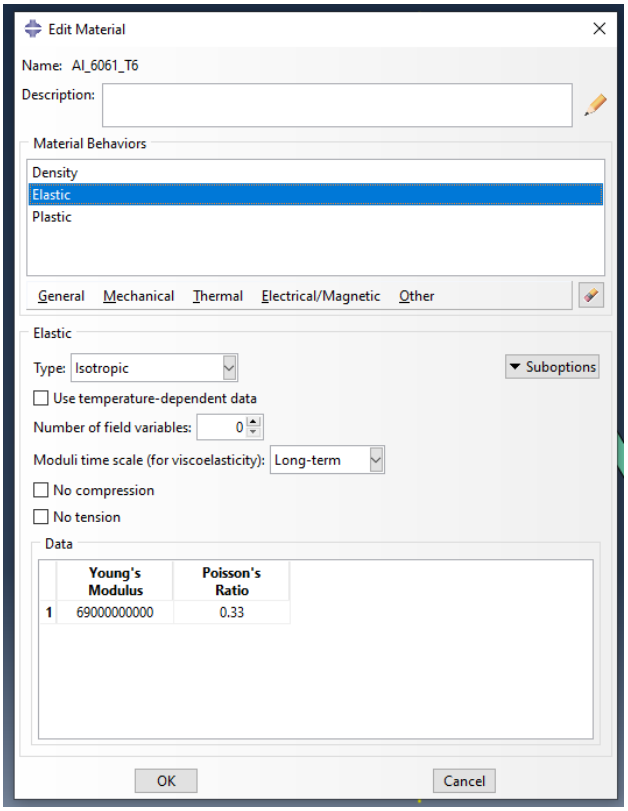

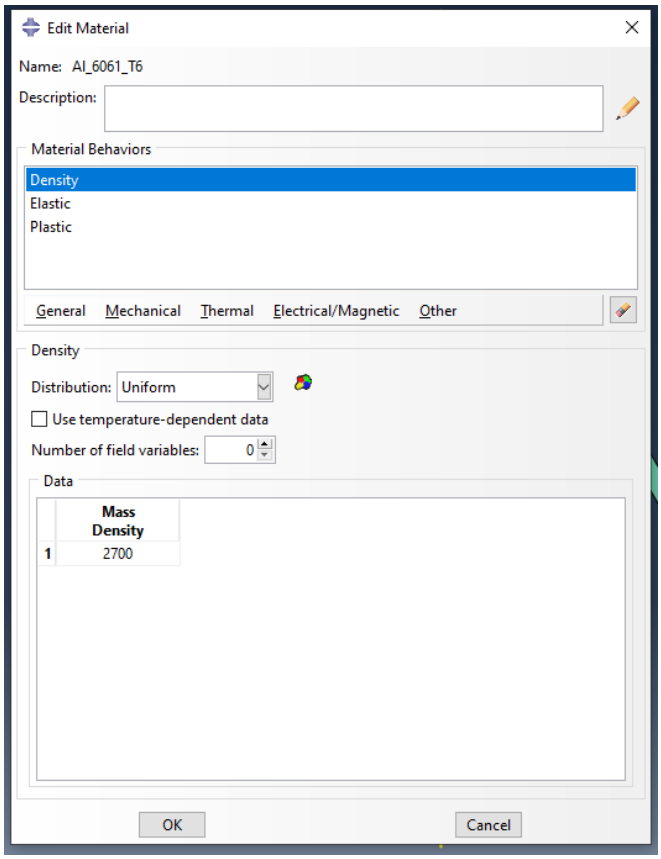

A-3 – Plastic Explosive 4 (PE4)

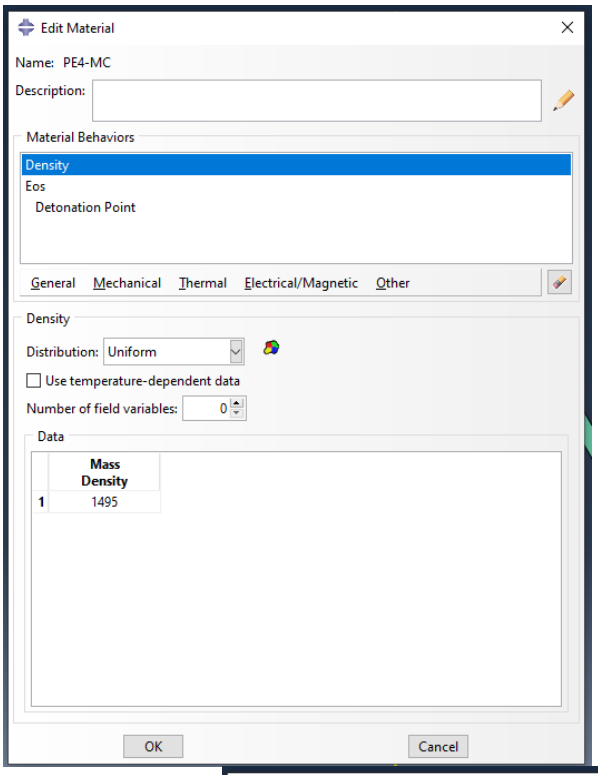

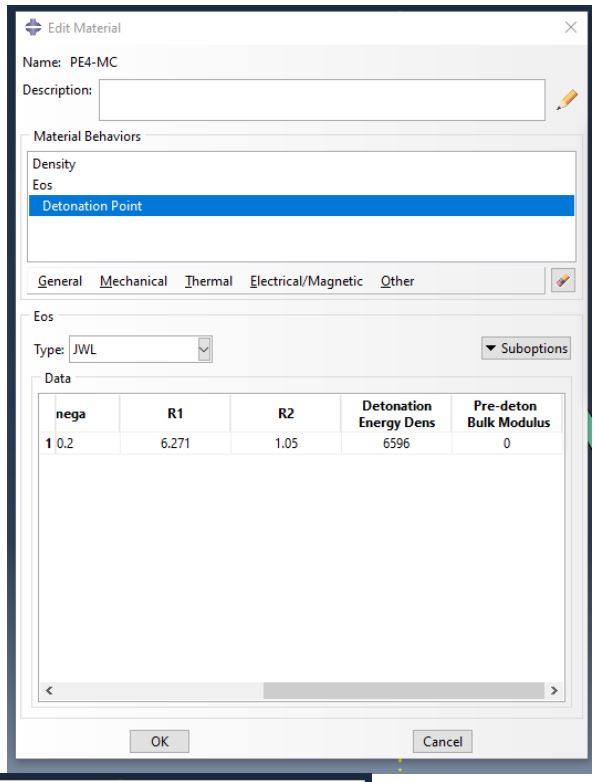

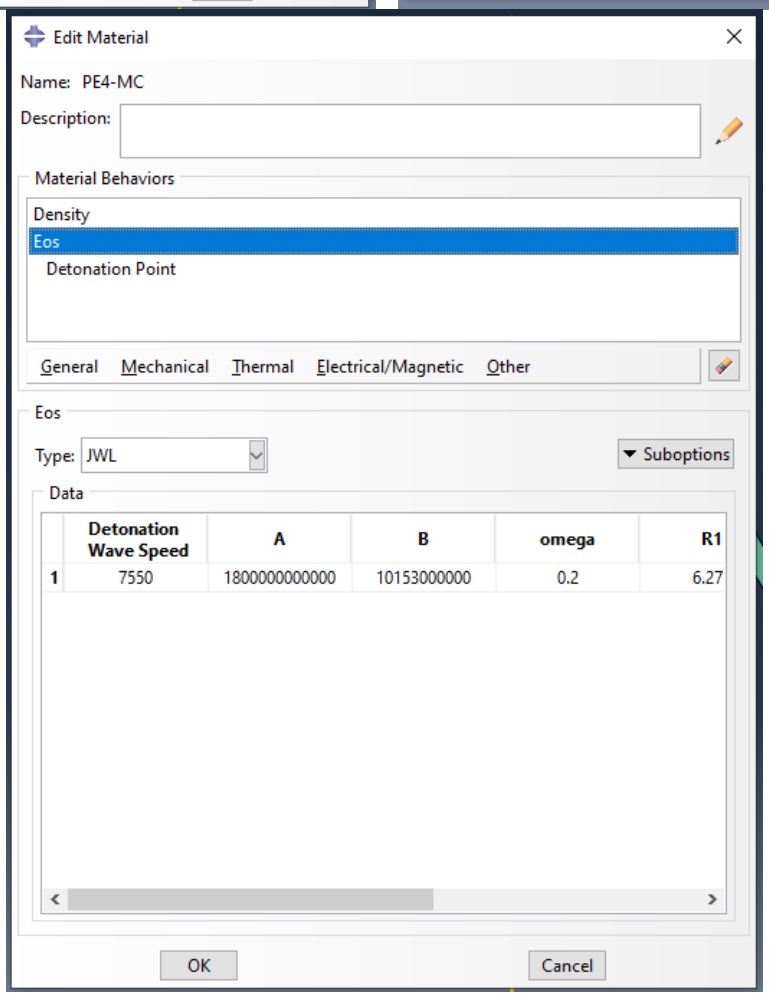

Appendix B – Technical Drawings

B-1 – Charge A

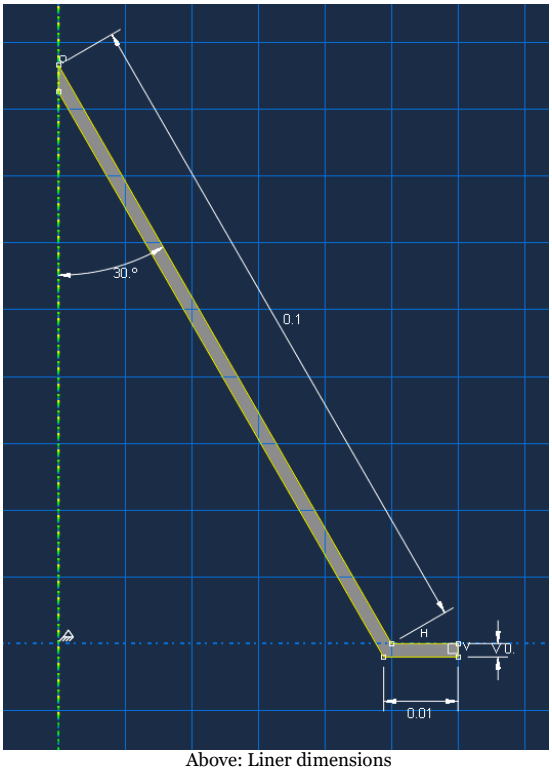

Above: Liner dimensions

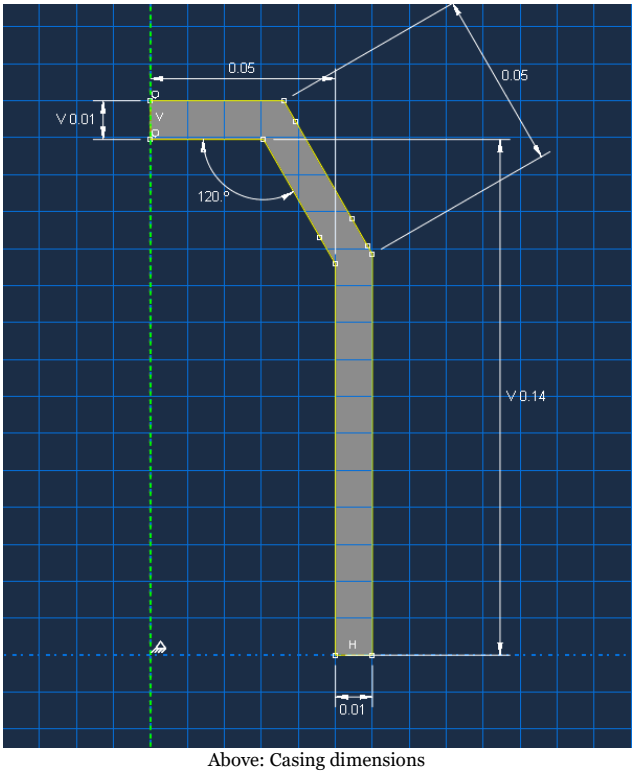

Above: Casing dimensions

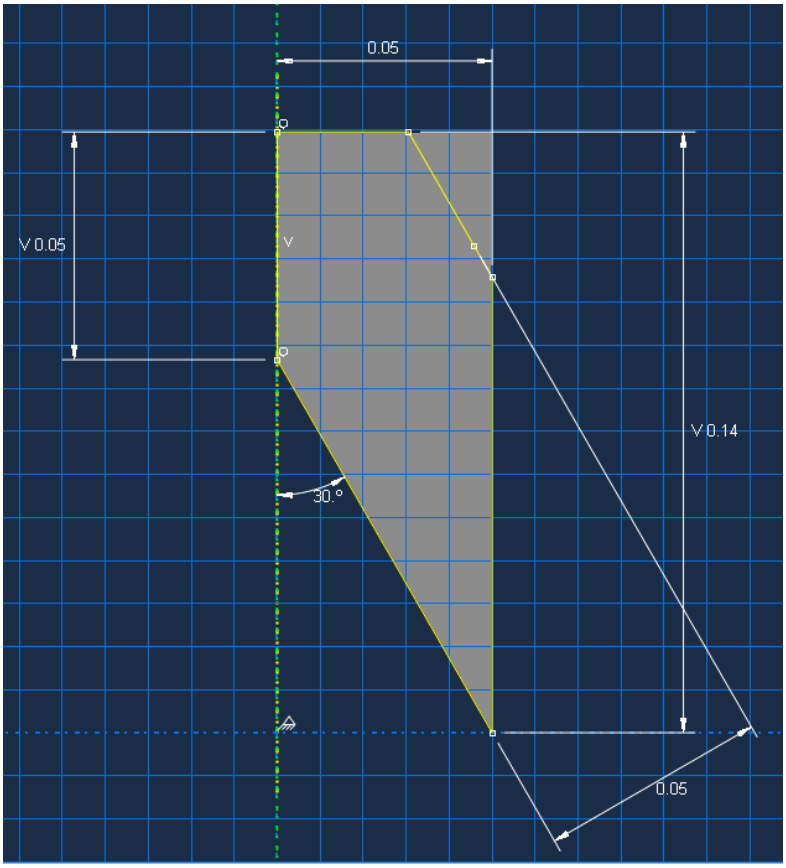

Above: HE Fill Dimensions

B-2 – Charge B

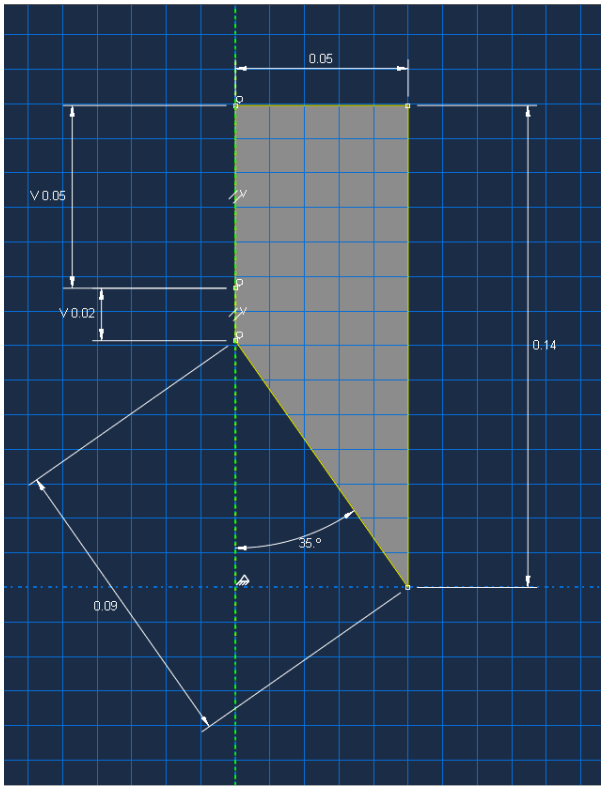

Above – HE Fill Dimensions

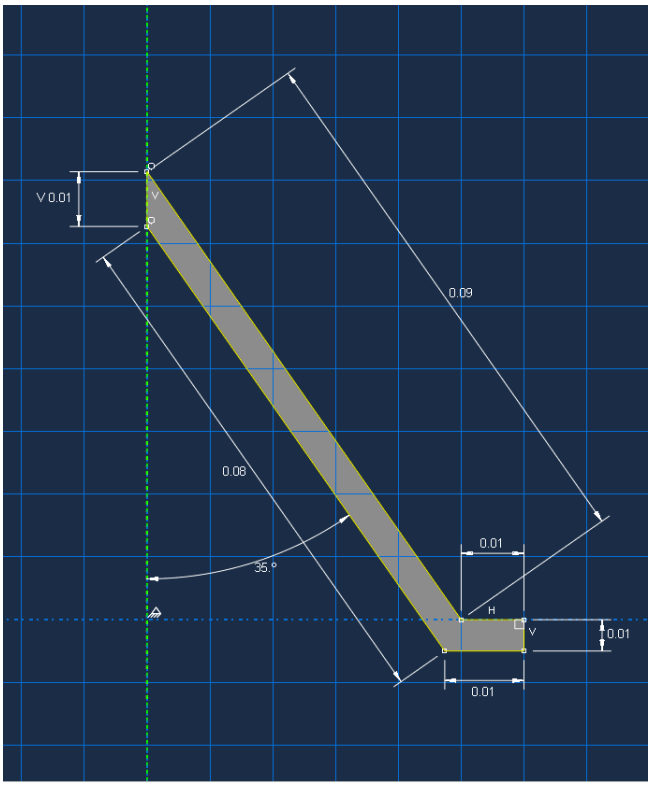

Above – Liner Dimensions

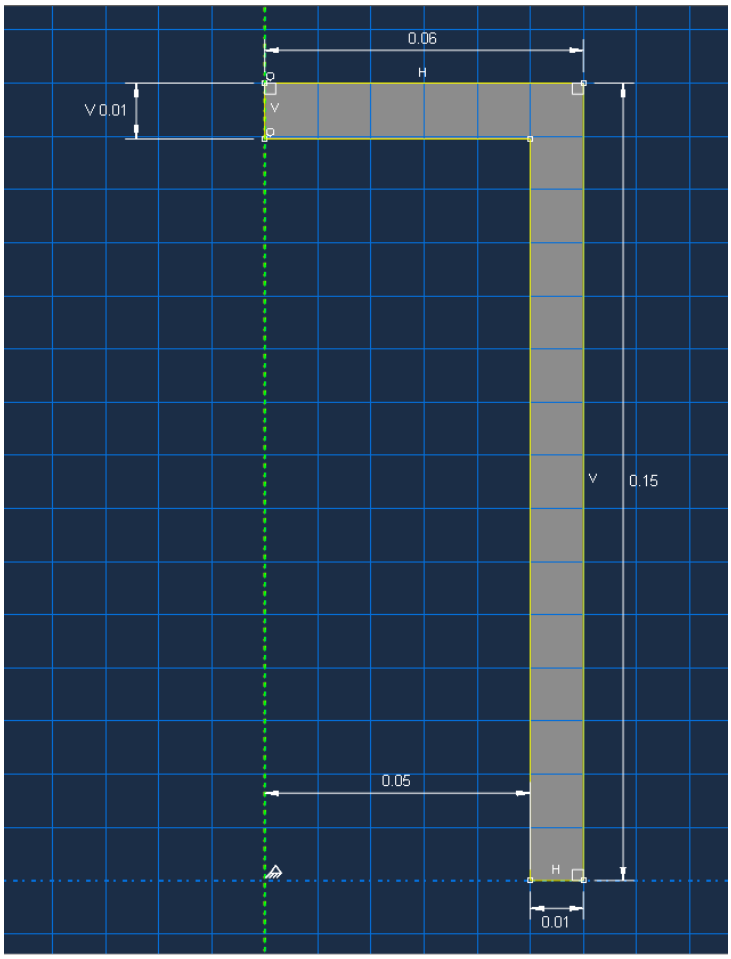

Above – Case Dimensions

Appendix C – Interaction Definition

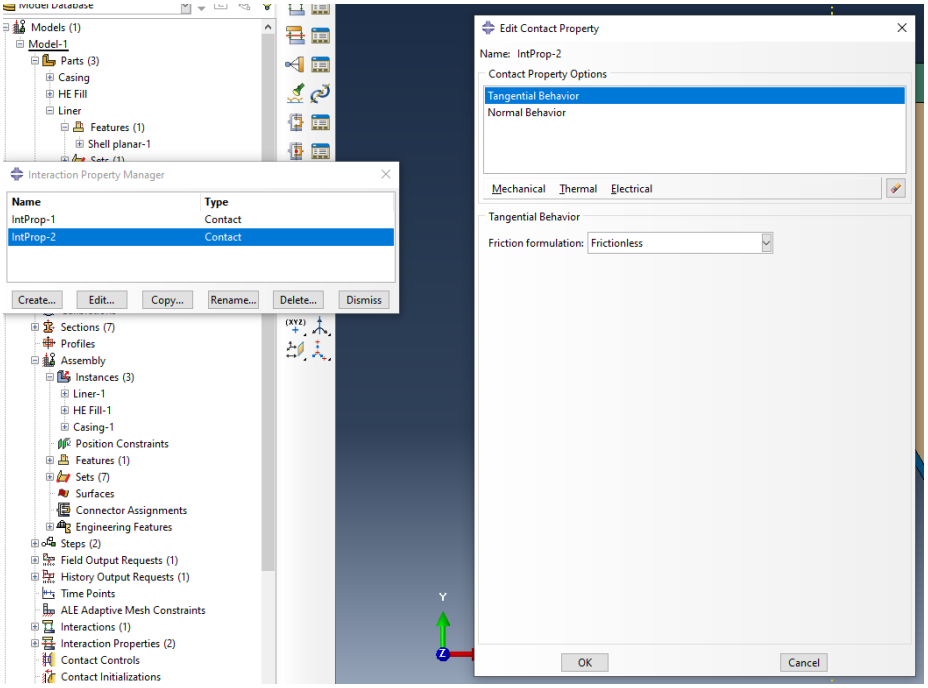

Above – Setting of Tangential Behaviour

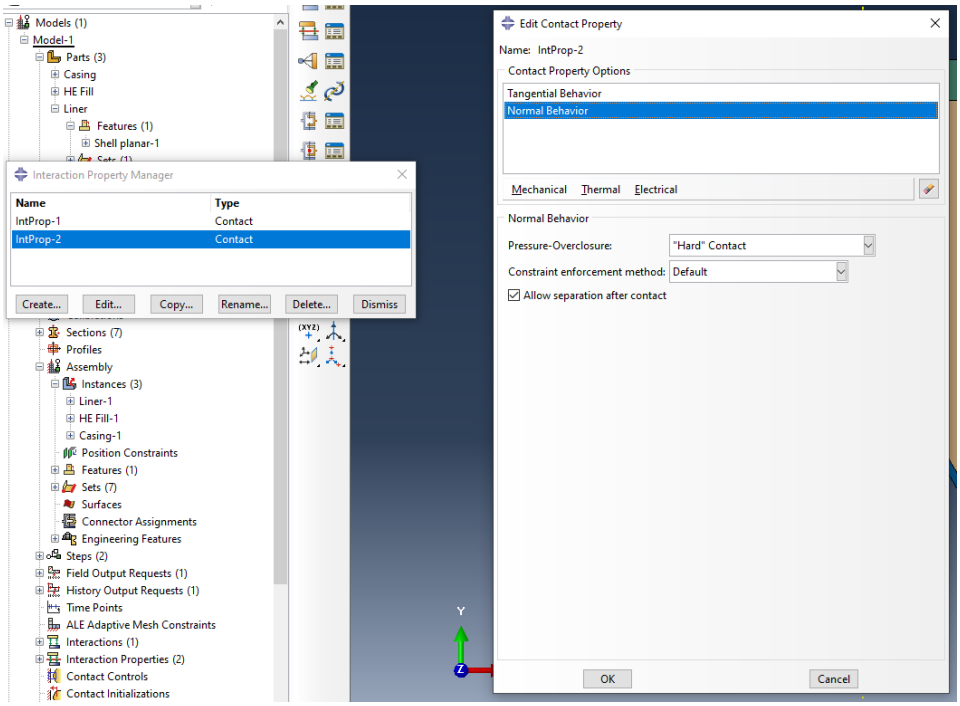

Above – Setting of normal behaviour

Appendix D – Charge 1, 2D Results

Visualisation		
Pressure	Jet Geometry	Smax, Principal
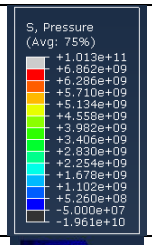	-	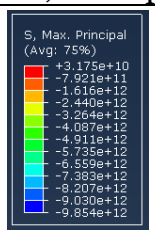
	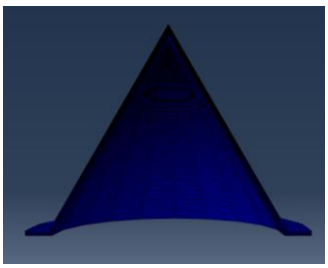	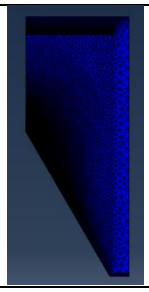
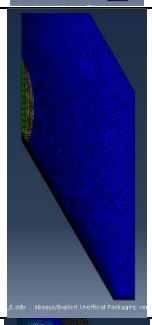	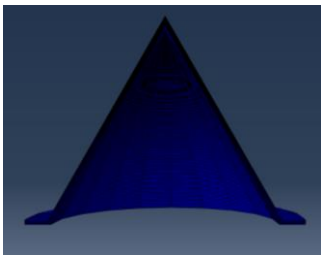	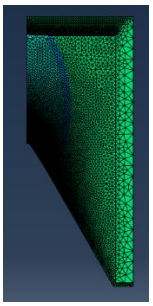
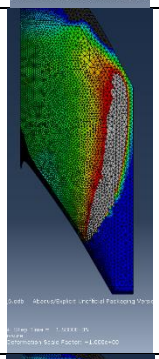	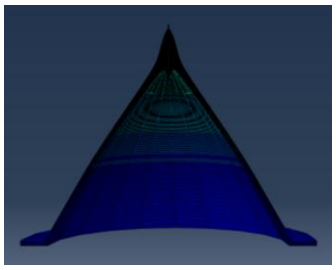	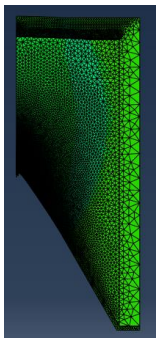
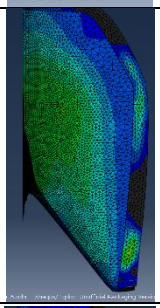	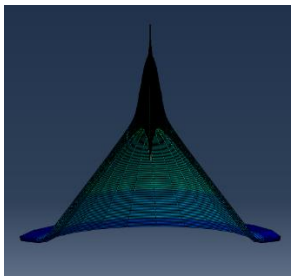	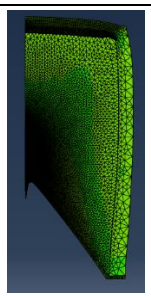
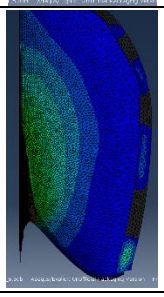	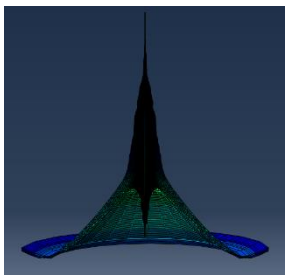	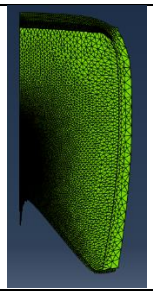

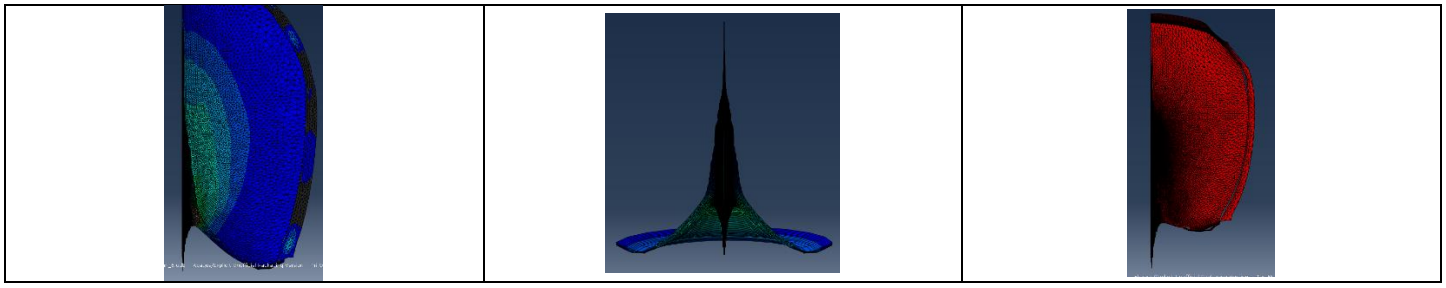

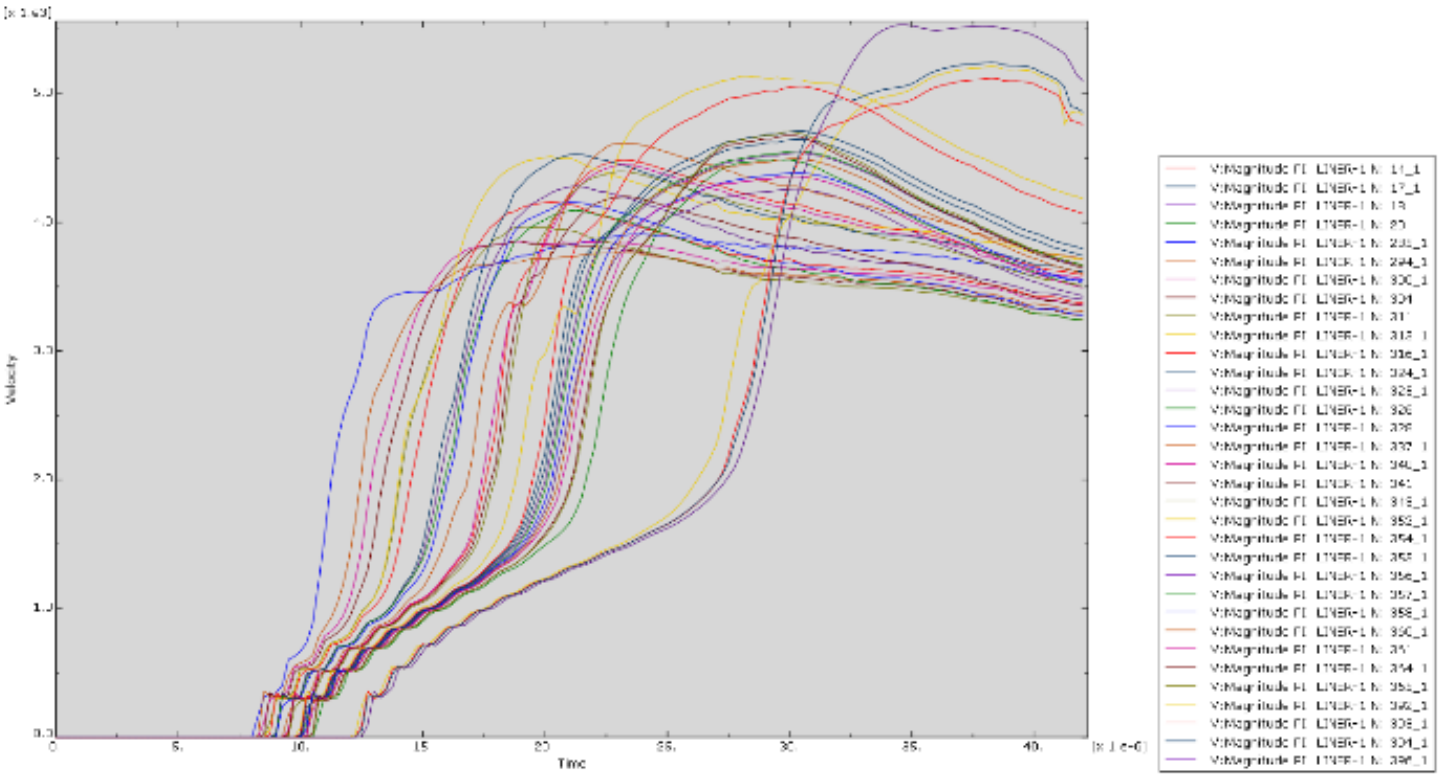

Above – Jet tip velocity, Charge 1, 2D.

Appendix E – Charge 2, 2D Results

Results: Charge 2, 2-Dimensional		
Pressure	Jet Geometry	Smax, Principal
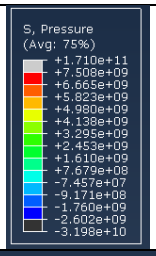		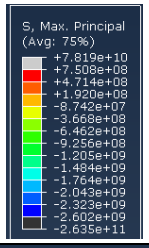
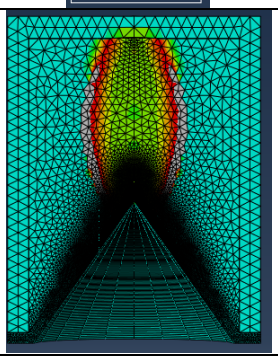	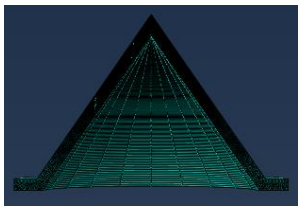	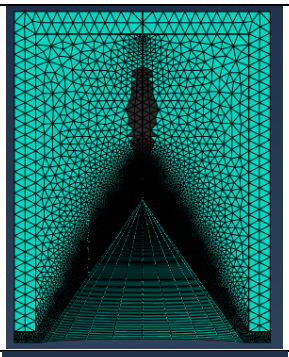
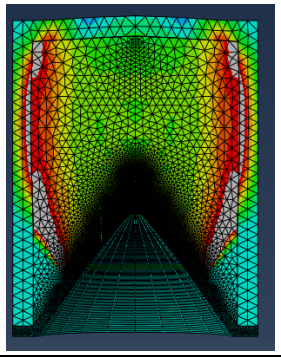	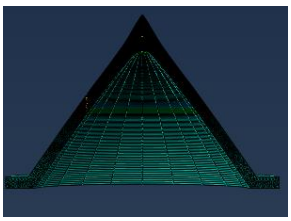	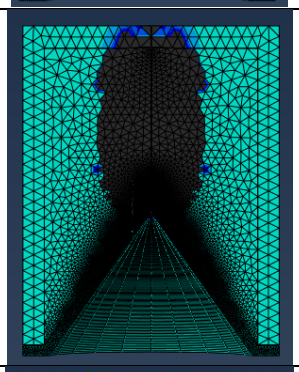
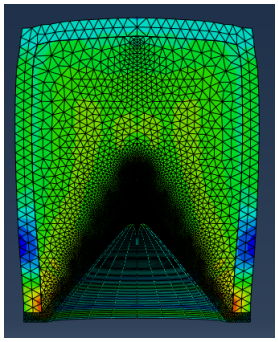	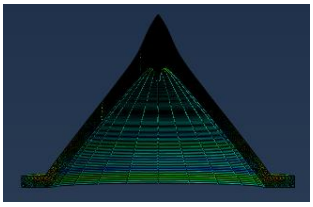	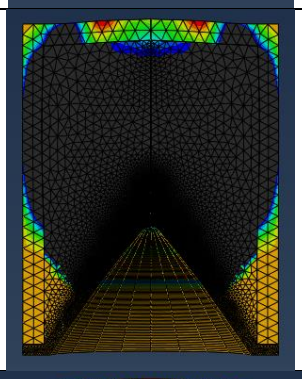
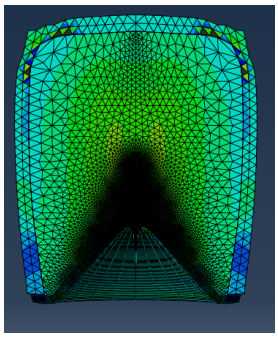	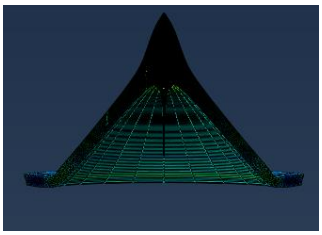	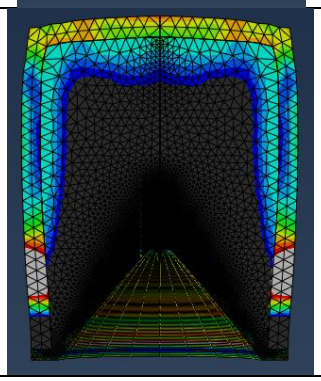

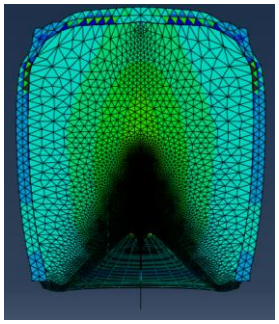	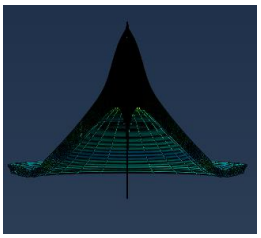	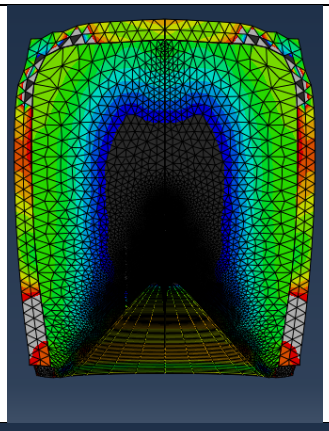
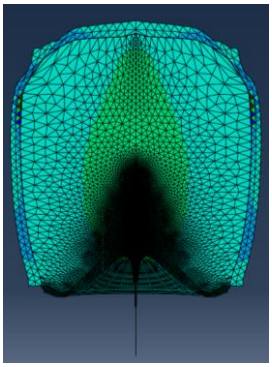	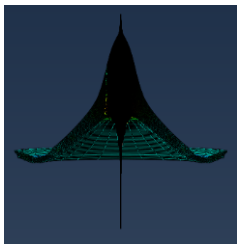	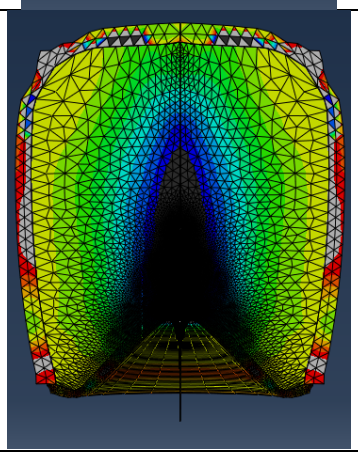
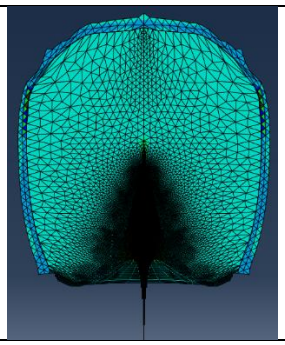		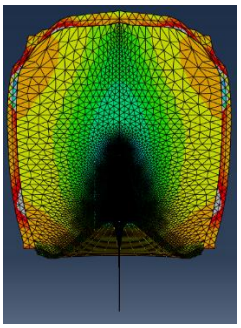
	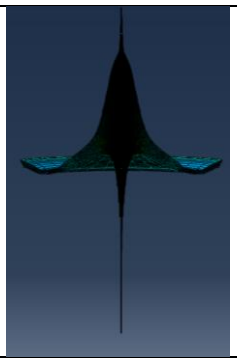	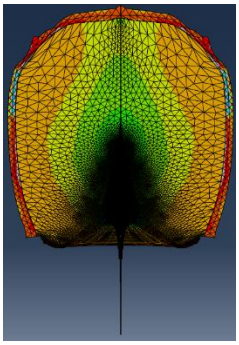

	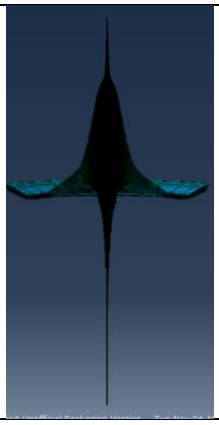	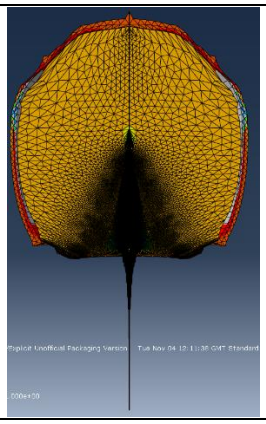

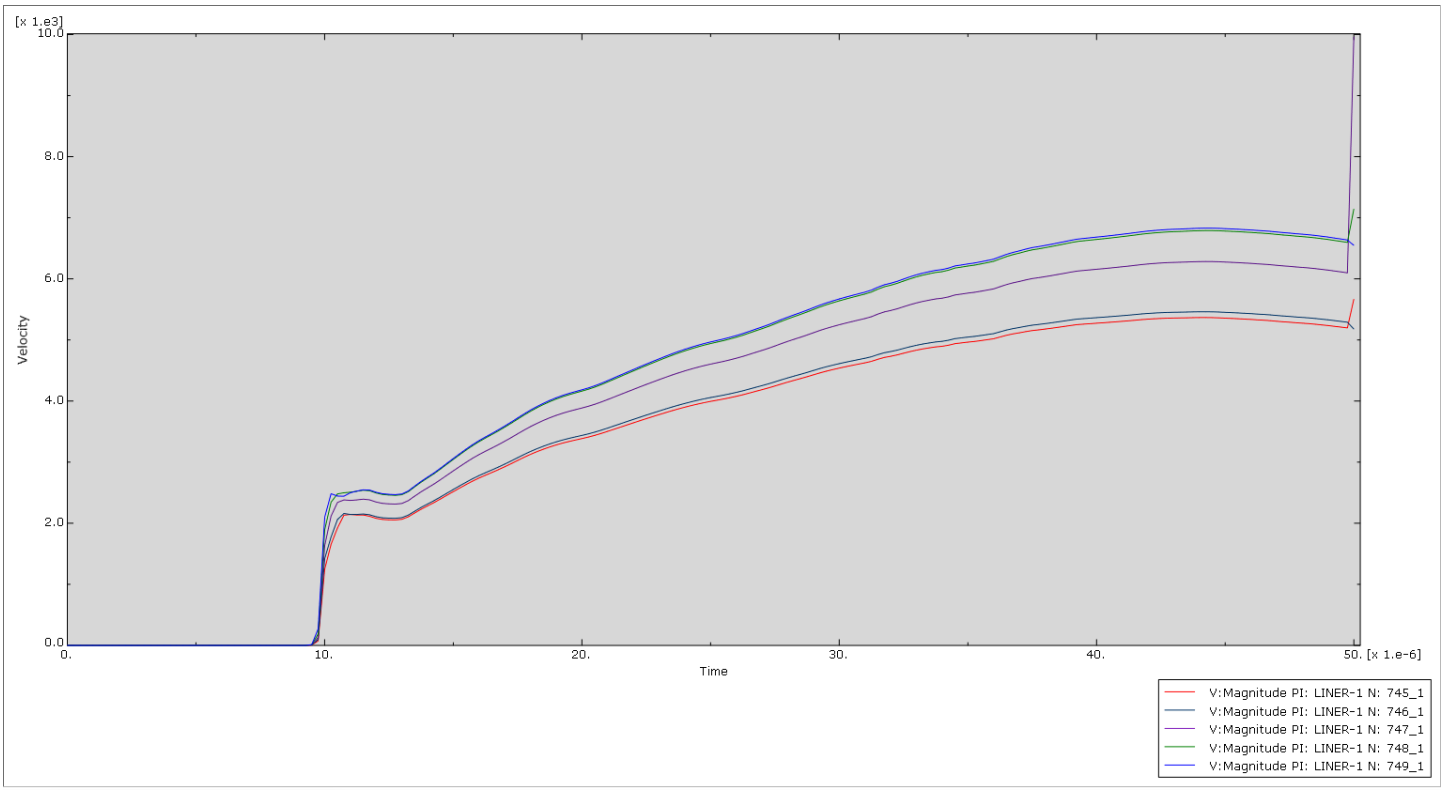

Above: Velocity plot, tip of jet.

Appendix F – Charge 2, 3D Results

Results: Charge 2, 3-Dimensional		
Pressure	Jet Geometry	Smax, Principal
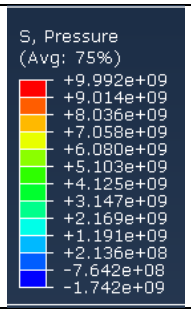	-	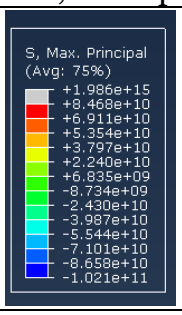
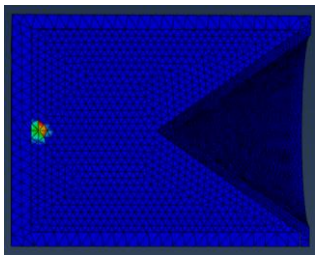	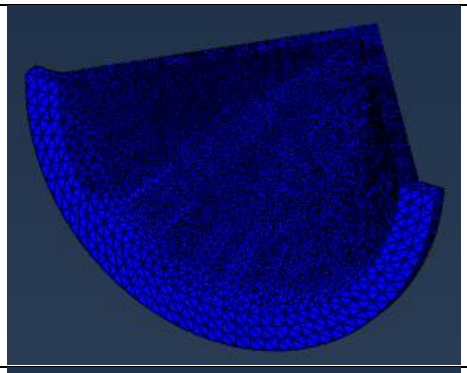	-
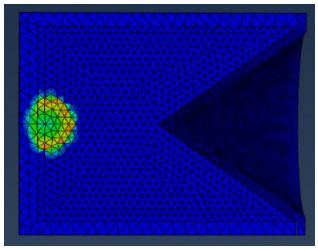	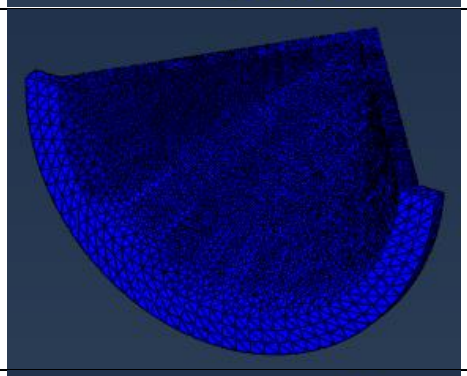	-
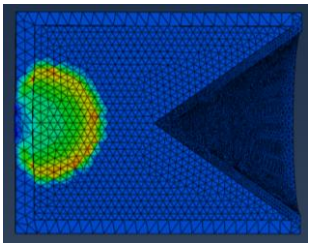	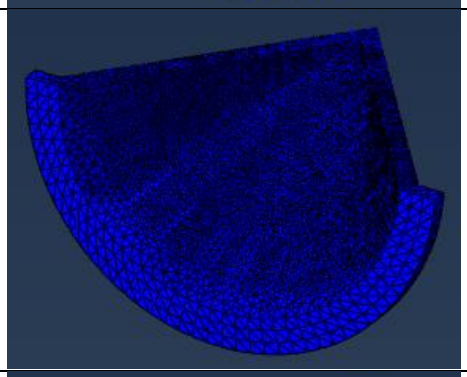	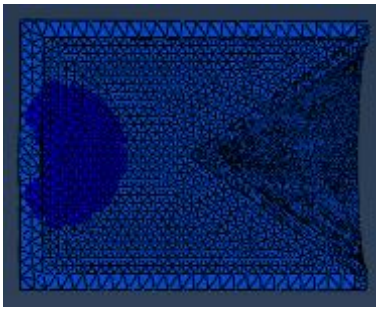
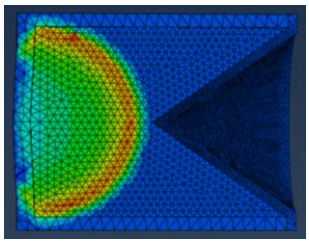	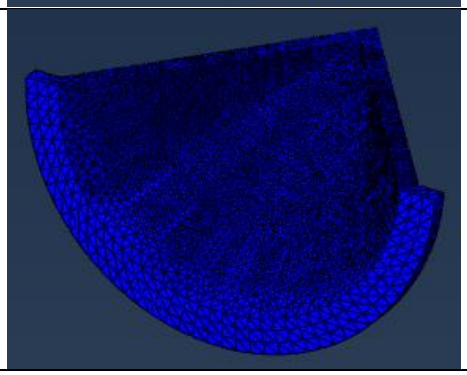	-

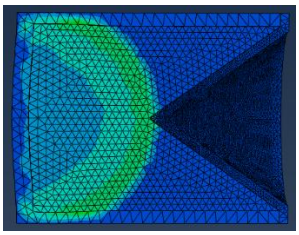	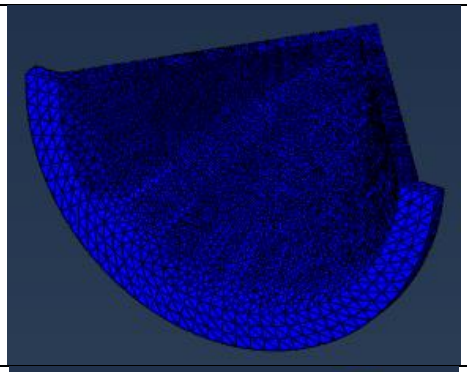	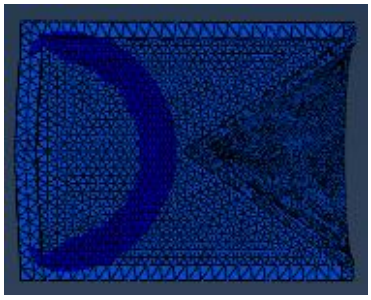
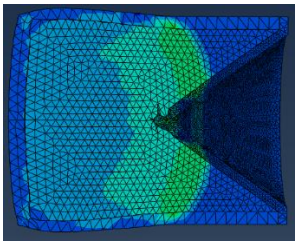	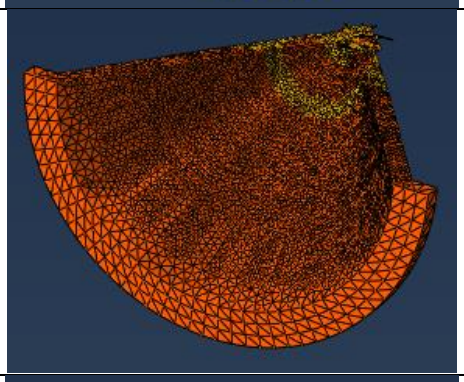	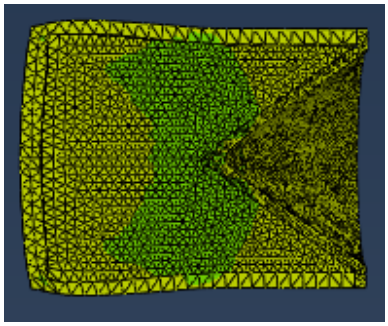
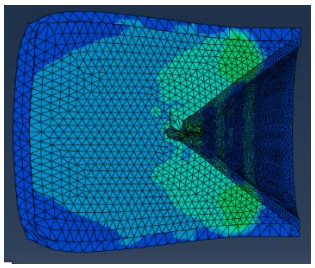	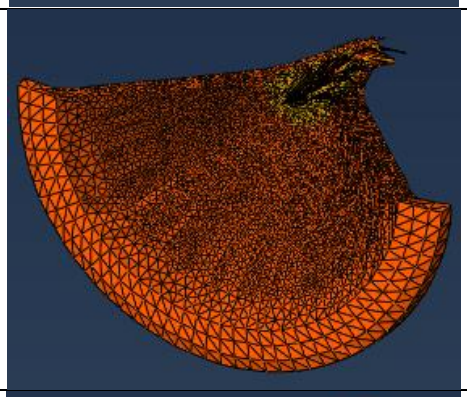	-
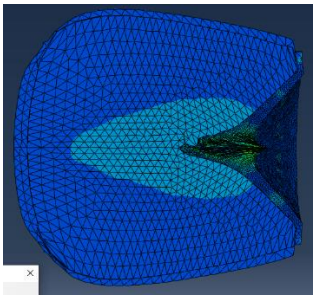	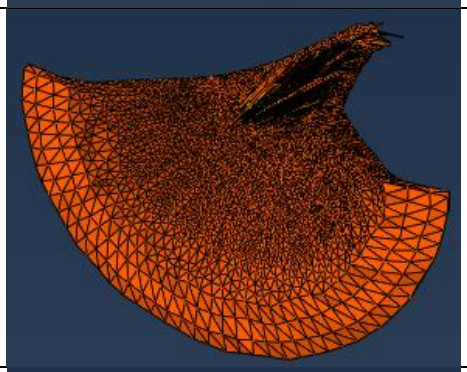	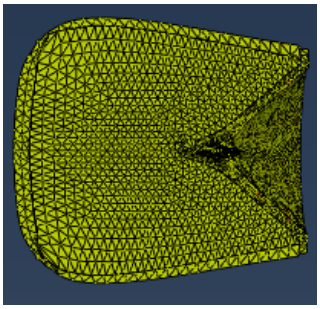
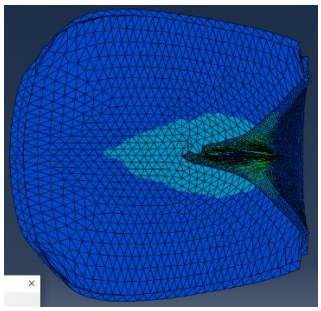	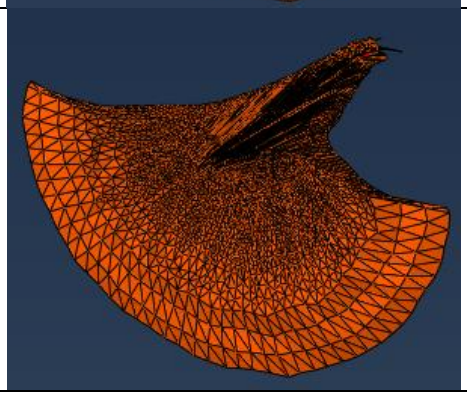	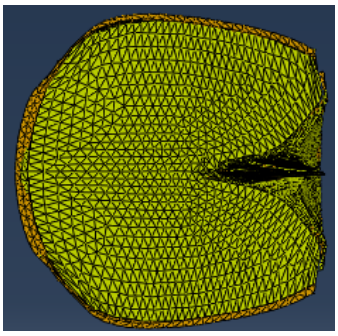

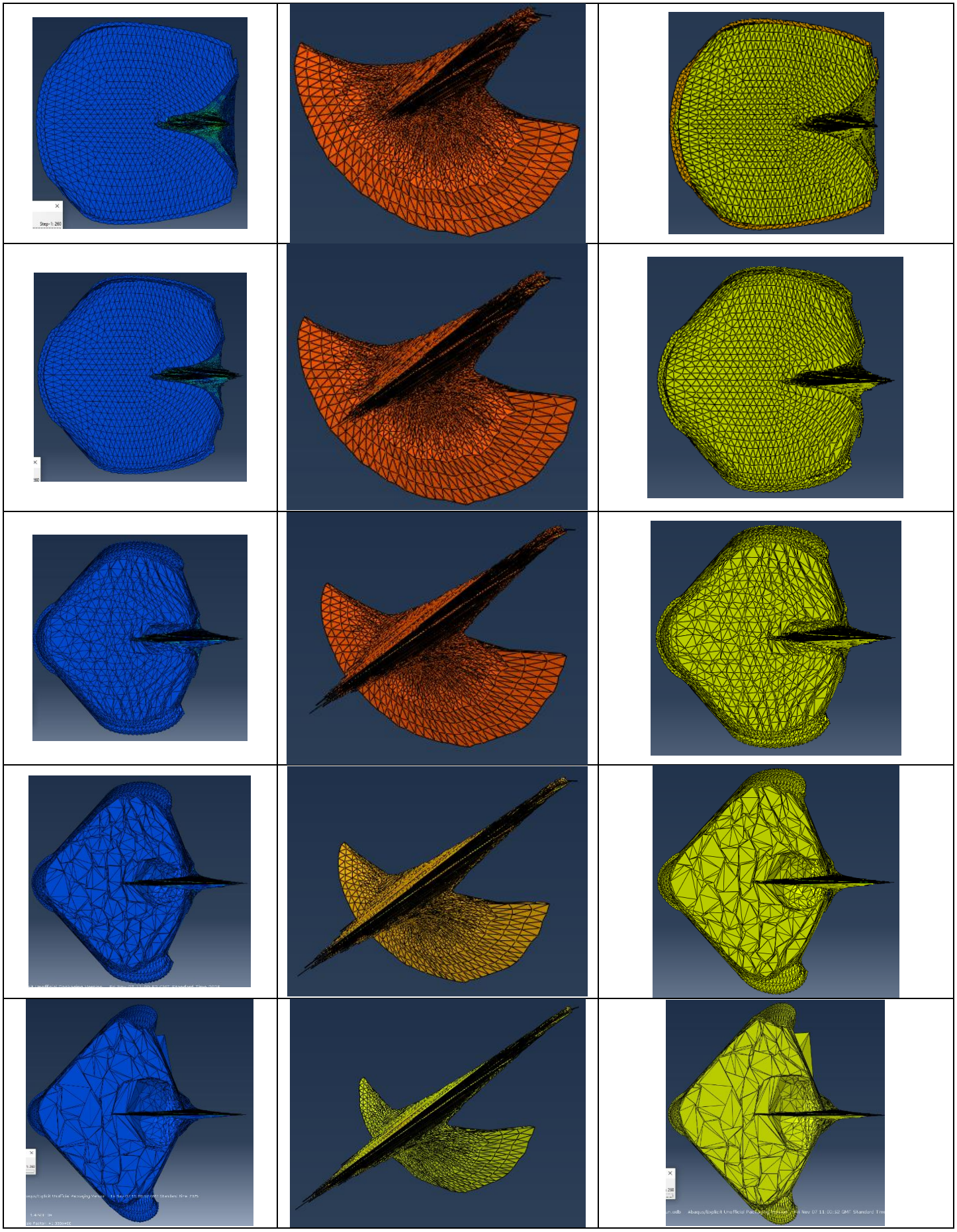

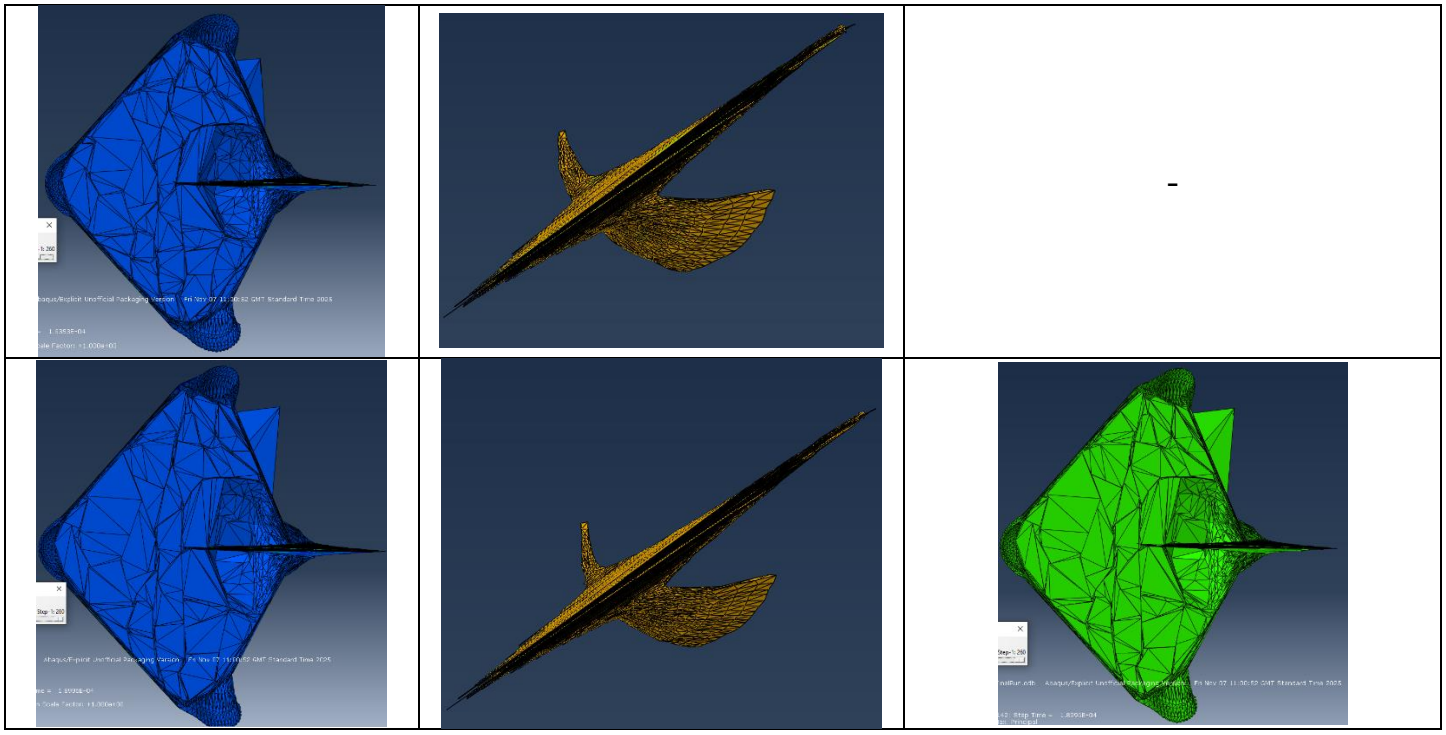

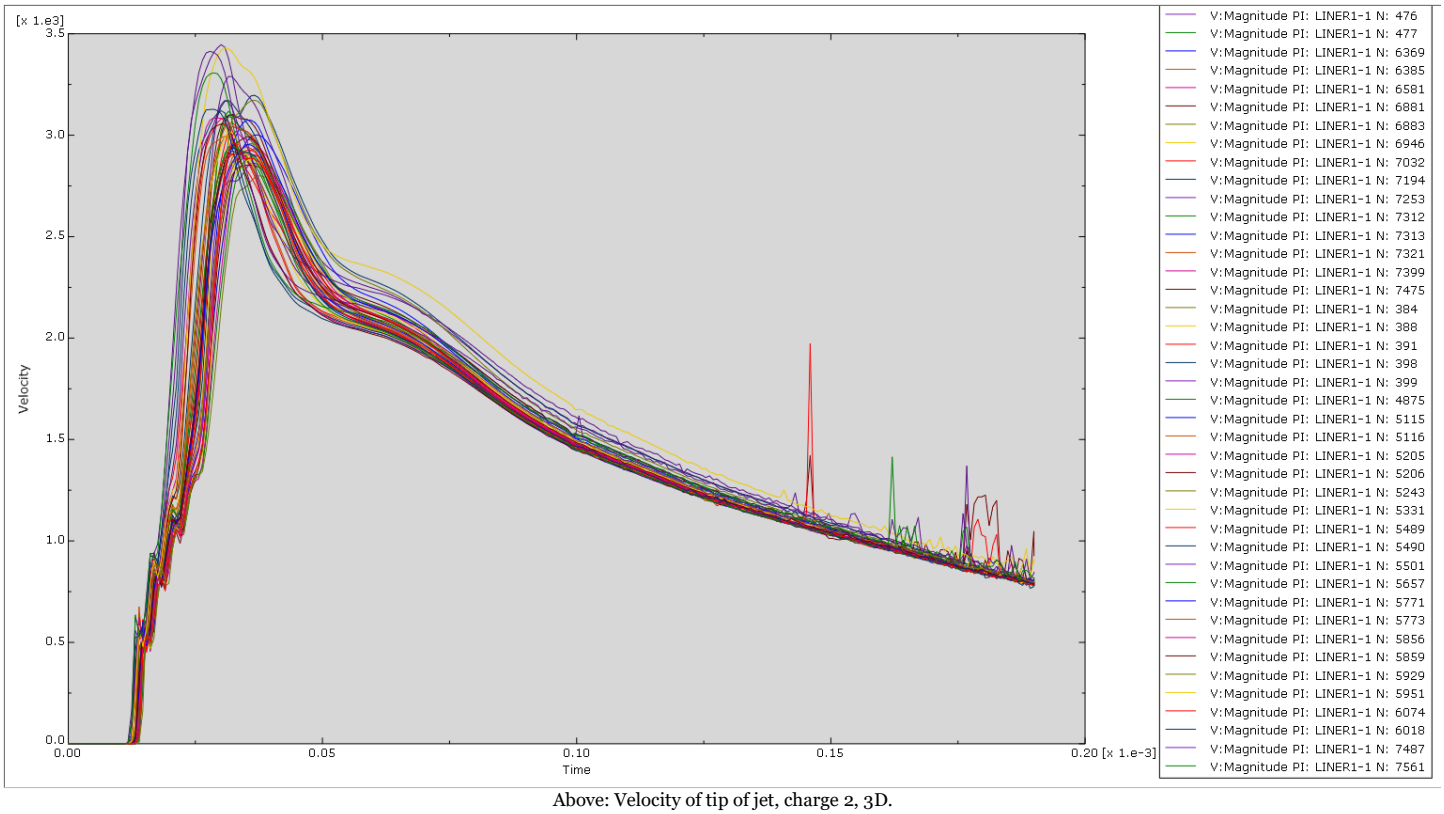

Above: Velocity of tip of jet, charge 2, 3D.